Palacký University Olomouc

Faculty of Science

Department of Cell Biology and Genetics

Generation of precision-cut of murine lung slice cultures for *ex vivo* assays

Master's Thesis

Bc. Samuel Herceg

Study programme: Biology

Field of Study: Molecular and Cell Biology

Form of Study: Full-time

Olomouc 2023   Supervisor: Mgr. Viswanath Das, Ph.D.

UNIVERZITA PALACKÉHO V OLOMOUCI
Přírodovědecká fakulta
Akademický rok: 2021/2022

ZADÁNÍ DIPLOMOVÉ PRÁCE
(projektu, uměleckého díla, uměleckého výkonu)

Jméno a příjmení: **Bc. Samuel HERCEG**
Osobní číslo: **R21926**
Studijní program: **N0511A030046 Molekulární a buněčná biologie**
Téma práce: **Generovanie presného rezu z kultúr myších pľúcnych rezov pre ex vivo testy**
Zadávající katedra: **Katedra buněčné biologie a genetiky**

Zásady pro vypracování

The preparation of tissue microslices for ex vivo experiments is a technique for producing organotypic slices with the use of a vibratome. Tissue slices are cost-effective and less time-consuming compared to in vivo experiments. This thesis will develop and optimise procedures for generating murine lung tissue slices for ex vivo experiments.

Rozsah pracovní zprávy:
Rozsah grafických prací:
Forma zpracování diplomové práce: **tištěná**
Jazyk zpracování: **Angličtina**

Seznam doporučené literatury:

1. Driehuis, E., Kretzschmar, K., & Clevers, H. (2020). Establishment of patient-derived cancer organoids for drug-screening applications. *Nature protocols, 15*(10), 3380–3409.
2. Vivarelli, S., Candido, S., Caruso, G., Falzone, L., & Libra, M. (2020). Patient-Derived Tumor Organoids for Drug Repositioning in Cancer Care: A Promising Approach in the Era of Tailored Treatment. *Cancers, 12*(12), 3636.
3. Nagle, P. W., Plukker, J., Muijs, C. T., van Luijk, P., & Coppes, R. P. (2018). Patient-derived tumor organoids for prediction of cancer treatment response. *Seminars in cancer biology, 53*, 258–264.

Vedoucí diplomové práce: **Mgr. Viswanath Das, PhD.**
Ústav molekulární a translační medicíny

Datum zadání diplomové práce: **27. října 2021**
Termín odevzdání diplomové práce: **31. července 2023**

doc. RNDr. Martin Kubala, Ph.D.
děkan

prof. RNDr. Zdeněk Dvořák, DrSc.
vedoucí katedry

V Olomouci dne 3. listopadu 2021

Bibliographical identification:

Author's name and surname	Samuel Herceg
Title	Generation of precision-cut of murine lung slice cultures for *ex vivo* assays
Type of thesis	Master
Department	Department of Cell Biology and Genetics
Supervisor	Mgr. Viswanath Das, Ph.D.
The year of defence	2023
Keywords	Precision-cut lung slices, respiratory disease, lung models, mouse
Number of pages	ix, 72
Language	English

Summary:

Respiratory diseases, such as COPD, lung cancer and respiratory infections, are ranked by the World Health Organization among the highest cause of mortality. Researchers have traditionally relied on cost-effective and easy-to-manipulate two-dimensional (2D) models to study these diseases, but these models have limitations in terms of physiological relevance. To address this issue, three-dimensional (3D) cell cultures have been developed, which more accurately replicate the complexities of tissue and organ microarchitecture and dynamic intracellular interactions. Despite the availability of 2D and 3D models, researchers cannot accurately replicate the spatial complexity and cellular richness of the lungs. Recently, more advanced three-dimensional models have been introduced, which can reflect the cellular richness and complexity of the lung – precision-cut lung slices (PCLS). PCLS are small, uniform, and generated from lung tissue, which retains most of the lung cell types, complex microarchitecture, anatomical structure, and responses to stimuli similar to native lungs. They allow testing a wide range of variables to replicate and reduce the required tissue or animals. We conducted the study to develop and optimise procedures for generating murine lung tissue slices with the use of vibratome for *ex vivo* experiments. Our results suggest that PCLS can be utilized for various *ex vivo* experiments, including immunofluorescence staining, lentiviral transduction, histological analysis, cytotoxicity or viability assays. This proves that PCLS are a suitable model that can be utilized for multiple experimental procedures to study drug discovery and respiratory disease mechanisms.

Bibliografická identifikácia:

Meno a priezvisko autora	Samuel Herceg
Názov práce	Generovanie presného rezu z kultúr myších pľúcnych rezov pre *ex vivo* testy
Typ práce	Diplomová
Pracovisko	Katedra bunkovej biológie a genetiky
Vedúci práce	Mgr. Viswanath Das, Ph.D.
Rok obhajoby práce	2023
Kľúčové slová	Presné pľúcne rezy, respiračné ochorenia, pľúcne modely, myš
Počet strán	ix, 72
Jazyk	Angličtina

Súhrn:

Respiračné ochorenia, ako CHOCHP, rakovina pľúc a respiračné infekcie, sú podľa Svetovej zdravotníckej organizácie jednou z najčastejších príčin úmrtnosti. Výskumníci sa pri štúdiu týchto ochorení tradične spoliehali na nákladovo efektívne a ľahko manipulovateľné dvojrozmerné (2D) modely, avšak tieto modely majú fyziologické obmedzenia. Aby sa tento problém vyriešil boli vyvinuté trojrozmerné (3D) bunkové kultúry, ktoré presnejšie replikujú zložitú mikroarchitektúru a dynamiku intracelulárnych interakcií tkanív a orgánov. Napriek dostupnosti 2D a 3D modelov, výskumníci nevedia presne replikovať priestorovú zložitosť a bunkovú rozmanitosť pľúc. Nedávno boli zavedené pokročilejšie trojrozmerné modely, ktoré môžu napodobniť bunkovú rozmanitosť a zložitosť pľúc – presné pľúcne rezy (PCLS). PCLS sú malé, jednotné a vznikajú z pľúcneho tkaniva, zachovávajú si väčšinu typov pľúcnych buniek, mikroarchitektúru, anatomickú štruktúru a reakcie na stimuly podobné natívnym pľúcam. Umožňujú testovanie širokého spektra premenných, tak aby sa zreplikovali a zredukovali požadované tkanivá alebo zvieratá. Štúdiu sme uskutočnili s cieľom vyvinúť a optimalizovať postupy na vytvorenie rezov myšacieho pľúcneho tkaniva na *ex vivo* experimenty s využitím vibratómu. Naše výsledky naznačujú, že PCLS je možné použiť na rôzne *ex vivo* experimenty, vrátane imunofluorescenčného farbenia, lentivírusovej transdukcie, histologickej analýzy, testov cytotoxicity alebo životaschopnosti. Je to dôkaz, že PCLS sú vhodným modelom, ktorý možno použiť na viaceré experimentálne postupy zamerané na objav liečiv a štúdium mechanizmov respiračných ochorení.

DECLARATION

I declare that this Master's Thesis was written independently under the guidance and help of my supervisor Mgr. Viswanath Das, Ph.D., using the cited literature listed in the references.

In Olomouc, ……………………   ……………………………

Bc. Samuel Herceg

ACKNOWLEDGMENT

This Master's thesis was performed at the Institute of Molecular and Translational Medicine in Olomouc, in collaboration with Palacký University in Olomouc.

Firstly, I would like to express my gratitude to my supervisor, Mgr. Viswanath Das, Ph.D., for his support and patience throughout the entire process of this thesis. His professional attitude and invaluable advice have been essential for shaping my research. I am also very grateful to Mgr. Narendran Annadurai for his encouragement and helpful attitude. Both of them taught me a set of new skills and techniques, advised me during experiments and helped me during times when I needed it the most, thank you. I would like to extend my appreciation to Mgr. Anna Janoštáková and Bc. Renata Buriánová for their kind approach and eagerness to assist me. Additionally, I am thankful to Mgr. Marta Khoylou Ph.D. for her invaluable aid in conducting histological experiments. I would also like to express my gratitude to the University Hospital in Olomouc for providing the drugs used during the experiments.

Finally, I must appreciate the strong support of my family, girlfriend, and friends during my studies. Their encouragement and support have been invaluable in helping me achieve my academic goals.

TABLE OF CONTENTS

LIST OF ABBREVIATIONS

2D	Two-dimensional
3D	Three-dimensional
3Rs	Refinement, Reduction and Replacement
AEC	Alveolar epithelial cells
ALI	Air-liquid interface
ALK	Anaplastic lymphoma kinase
ALRTI	Acute lower respiratory tract infections
ASCs	Adult stem cells
ATCC	American Type Culture Collection
BRAF	Serine/threonine-protein kinase B-Raf
CAP	Community-acquired pneumonia
COPD	Chronic obstructive pulmonary disease
CREBBP	Cyclic adenosine monophosphate response element binding protein
CXCL(x)	The chemokine (C-X-C motif) ligand (x)
DDR2	Discoidin domain receptor tyrosine kinase 2
ECM	Extracellular matrix
EGFR	Epidermal growth factor receptor
FcεRI	High-affinity IgE receptor
FGFR(x)	Fibroblast growth factor receptor (x)
G-CSF	Granulocyte colony-stimulating factor
GM-CSF	Granulocyte-macrophage colony-stimulating factor
GNAS	Guanine nucleotide-binding protein, and alpha stimulating activity polypeptide
HAP	Hospital-acquired pneumonia
HBEC	Human bronchial epithelial cells
HER2	Human epidermal growth factor receptor 2
HIV	Human immunodeficiency virus
IFN-α	Interferons of type I
IFN-γ	Interferon-gamma
IFN-λ	Interferons of type III
IgE	Immunoglobulin E

IL(x)	Interleukin (x)
ILC2s	Innate lymphoid cells type 2
iPSC	Induced pluripotent stem cells
JAK(x)	Janus kinase-(x)
KRAS	Kirsten rat sarcoma viral oncogene homolog
LOC	Lung-on-a-chip
NF-κB	Nuclear factor kappa B
NSCLC	Non-small-cell lung cancer
PCLS	Precision-cut lung slices
PDMS	Polydimethylsiloxane
PI3K	Phosphoinositide-3-kinase
PSCs	Pluripotent stem cells
PTEN	Phosphatase and tensin homolog
ROS	Reactive oxygen species
ROS1	ROS proto-oncogene 1, receptor tyrosine kinase
RSV	Respiratory syncytial virus
SARS–CoV-2	Severe acute respiratory syndrome coronavirus 2
SCLC	Small-cell lung cancer
TB	Tuberculosis
Th(x)	Helper T lymphocytes type (x)
TNF	Tumour necrosis factor
TRPV4	Transient receptor potential cation channel subfamily V member-4

x = number

LIST OF FIGURES

LIST OF TABLES

1 INTRODUCTION

Respiratory diseases, including COPD and respiratory infections, are a leading cause of morbidity after heart disease, stroke, and cancer, according to statistical data from the World Health Organization (2020). Despite significant financial investment in research and development of treatments, the prevalence of crucial respiratory diseases such as COPD, cancer, idiopathic pulmonary fibrosis, and asthma has remained constant or even increased (Liu et al., 2019). The COVID-19 pandemic has further highlighted the importance of accelerating fundamental research of respiratory diseases and lung biology and developing technologies and models for optimized diagnosis and treatment strategies (Viana et al., 2021).

Traditionally, respiratory researchers have relied on basic two-dimensional cellular models, which are affordable but have several limitations. Recently, more advanced three-dimensional models have been introduced to overcome these limitations, but some of these models are unable to reflect the cellular richness and complexity of the lung. Additionally, the low availability of human tissues and the implementation of the 3Rs principles to reduce animal usage have led to the introduction of precision-cut lung slices. These slices define tissue sections of uniform thickness, generated from a single piece of tissue, and can be obtained from various organs or animals. This allows for testing a wide range of variables in replicate, further reducing the amount of source tissue or animals required (Liu et al., 2019; Viana et al., 2021).

2 AIMS OF THE THESIS

This thesis aims to develop and optimise procedures for generating murine lung tissue slices with the use of vibratome for *ex vivo* experiments and test the suitability of the generated murine precision-cut lung slices as an experimental model using the transduction, cytotoxic assays and immunofluorescence staining.

3 LITERATURE REVIEW

3.1 The most prevalent respiratory diseases

According to the National Cancer Institute of the United States (n.d.) and the National Institute of Environmental Health Sciences of the United States (n.d.), respiratory diseases are illnesses that affect the lungs and other parts of the respiratory system, preventing them from functioning correctly. Lungs are internal organs regularly exposed to the outside environment, which consists of organic and inorganic pollutants or biological agents, risking the development of respiratory diseases (Shukla *et al*., 2020). Respiratory diseases can be broadly divided into communicable diseases, including infectious diseases of the lungs, such as pneumonia and tuberculosis, and noncommunicable diseases not caused by infectious agents, such as chronic obstructive pulmonary disease (COPD), asthma and lung cancer (Shukla *et al.*, 2020). These diseases were listed in the Global Impact of Respiratory Diseases report as the "Big Five", making them the most common causes of severe illnesses and deaths worldwide (Forum of International Respiratory Societies, 2021). This statement is confirmed by World Health Organisation (2020) data, according to which three out of the top ten causes of death were caused by respiratory diseases in 2019, leading to more than 8 million deaths annually. Additionally, air pollution caused by industrialization and globalization will likely be a major global concern in the coming years (Rehman *et al*., 2019; Elbarbary *et al*., 2020). Therefore, research focusing on respiratory diseases will be important to improve respiratory disease prevention, diagnosis and management, which might lead to fewer deaths (Cohen *et al.*, 2022).

3.1.1   Chronic obstructive pulmonary disease (COPD)

COPD is a preventable and treatable disease characterized by airflow limitation that is difficult to reverse (Rabe *et al.*, 2007). This airflow limitation is caused by chronic bronchiolitis and emphysema, defined by the destruction of the lung parenchyma and expansion of alveoli size resulting from chronic inflammation. In many cases, hypersecretion of mucus is also a pathological feature of COPD (Barnes *et al.*, 2015; Chronic Obstructive Lung Disease, Global Initiative for., 2017). This inflammation is most commonly located in peripheral airways or lung parenchyma and increases during acute exacerbations (Gan, 2004). As a result of this chronic inflammation, components of both innate and adaptive immunity, such as macrophages, B-lymphocytes, T-lymphocytes, and neutrophils, are increased, in addition to activating airway and alveolar epithelial cells, endothelial cells, and fibroblasts. The cooperation between

adaptive and innate immunity is mediated by dendritic cells (Steinman and Banchereau, 2007; Barnes, 2008; Barnes 2014). The inflammation associated with COPD is highly amplified, yet the exact mechanism of this amplification remains unclear (Barnes, 2014). The most common risk factors of COPD, which cause this chronic inflammation, are the inhalation of tobacco smoke, air pollutants, and genetic predispositions, such as cutis laxa and α1-antitrypsin deficiency (Barnes *et al.*, 2015; Chronic Obstructive Lung Disease, Global Initiative for., 2017). Tobacco smoke and other air pollutants activate surface macrophages and airway epithelial cells, triggering the release of inflammatory mediators and attracting neutrophils, monocytes, and lymphocytes into the lungs. The most common chemokines released by epithelial cells are tumour necrosis factor (TNF) alpha, interleukin (IL)-1 beta, and CXCL8 (IL-8). Macrophages also release other inflammatory mediators and elastolytic enzymes, such as the highly prevalent MMP-9. The macrophage elastolytic enzymes and neutrophil elastase, produced by neutrophils, degrade the extracellular matrix of the lung parenchyma, resulting in emphysema (Russell *et al.,* 2002; Donelly and Barnes, 2006; Barnes, 2014). Additionally, epithelial cells, alongside macrophages and neutrophils, produce reactive oxygen species (ROS), which activate nuclear factor kappa B (NF-κB), leading to the activation of more inflammatory genes (Tomita *et al.*, 2003).

Epidemiological statistics show that in 2019, approximately 200 million people were afflicted with COPD (Meghji *et al.*, 2021), with 3.23 million fatalities reported by the World Health Organization (2022), making it the third leading cause of death in the world. In Europe, respiratory disease has been identified as the third leading cause of death, with COPD accounting for 40% of all deaths due to respiratory diseases (Lindberg *et al*., 2021). The annual mortality rate of COPD in the Czech Republic is 3500 cases per 10.6 million people, representing a considerable burden on the population (Brat *et al.*, 2021).

3.1.2   Asthma

Asthma is a chronic inflammatory disease of the conducting airways. This inflammation, caused by the combined activity of innate and adaptive immune cells and epithelial cells in the airways, leads to increased mucus production, airway wall remodelling, and hyperactivity of the bronchi. In patients, this can manifest as chest tightness, shortness of breath, and wheezing (Lambrecht and Hammad, 2014; Hammad and Lambrecht, 2021). According to Suraya *et al.* (2021), asthma can be divided into two groups based on molecular mechanisms: type 2 and non-type 2.

In type 2 asthma, after phagocytosis of the antigen by dendritic cells or macrophages, the antigen is presented to naïve T cells, which further differentiate into type 2 helper T lymphocytes (Th2) that produce Th2 cytokines (Gordon *et al.*, 2016; Peters *et al.*, 2018). This type of bronchial asthma is characterized by the elevated production of Th2 cytokines, mainly interleukin-4 (IL-4), IL-5, and IL-13 (Peters and Wenzel, 2020). Th2 cytokines are not only produced by Th2 cells but also by basophils, mast cells, and type 2 innate lymphoid cells (ILC2s). Th2 cells, through Th2 cytokines, stimulate the production of immunoglobulin E (IgE) by B lymphocytes. IgE antibodies then bind to mast cells' high-affinity IgE receptor (FcεRI), triggering the release of various mediators such as histamine, leukotrienes, and prostaglandins (Shapouri-Moghaddam *et al.*, 2018; Suraya *et al.*, 2021). These mediatory molecules stimulate mucus production and bronchial hyperactivity and recruit other inflammatory lymphocytes, including neutrophils, eosinophils, and lymphocytes (Suraya *et al.*, 2021).

Non-type 2 asthma is closely connected to neutrophilic inflammation. However, the proper mechanism of recruiting neutrophils is not fully understood. After contact with tobacco smoke or other irritants, toll-like receptors become activated, and the recruitment of Th1 and Th17 occurs (Saeki *et al.*, 219; Suraya *et al.*, 2021). Th1 produces cytokine interferon-gamma (IFN-γ), whereas Th17 cells release IL-17 A and IL-17 F to attract neutrophils into the lungs, leading to elevated inflammation and airway remodelling, local airway tissue injury and broncho-constriction. CXCL8 might directly activate neutrophils or indirectly with the help of IL-6, granulocyte colony-stimulating factor (G-CSF), granulocyte-macrophage colony-stimulating factor (GM-CSF), IL-8, the chemokine (C-X-C motif) ligand 1 (CXCL1), and CXCL5 secreted by airway epithelial cells (Agache and Akdis, 2016; Carr *et al.*, 2018).

Asthma is a chronic disease affecting adults and children, with later being affected more. According to the Global Asthma Report 2022 (2022), asthma affected 262 million people in 2019 and killed over 461 000 individuals.

3.1.3 Acute lower respiratory tract infections

Acute lower respiratory tract infections (ALRTI) are caused by lower respiratory tract infections, which lead to an obstruction of the bronchial system (Correia *et al.*, 2021). According to European Lung Foundation (2021), the significant causes of ALRTI are pneumonia, acute bronchitis and bronchiolitis.

Pneumonia affects the alveoli and distal bronchial system of the lungs. Pneumonia is divided into two major groups: community-acquired pneumonia (CAP) and hospital-acquired

pneumonia (HAP; Torres *et al.*, 2021). It is caused by microorganisms such as bacteria, viruses and fungi. The representation of these microorganisms differs in CAP and HAP. In CAP, the most prevalent are bacteria *Streptococcus pneumoniae, Mycoplasma pneumoniae, Legionella pneumophila* and respiratory viruses such as *Haemophilus influenzae*. Instead, HAP includes bacteria *Staphylococcus aureus*, Enterobacterales (for example, *Pseudomonas aeruginosa*) and Acinetobacter spp. (Cilloniz *et al.*, 2011; Torres *et al.*, 2017). These pathogens can spread quickly via aerosols or direct contact (Kutter *et al.*, 2018). Mutant pathogens evade immune clearance and transit from colonization to infection (Torres *et al.*, 2021).

Acute bronchitis is characterized as an acute inflammation of the large airways and trachea, without pneumonia, accompanied by a cough (Wenzel and Fowler, 2006; Kinkad and Long, 2016). It is mainly caused by viral infections, including rhinovirus, enterovirus, influenza A and B, parainfluenza, coronavirus, human metapneumovirus, and respiratory syncytial virus. However, in 1 to 10% of the cases of acute bronchitis, bacteria, such as *Mycoplasma pneumoniae, Streptococcus pneumoniae, Haemophilus influenzae, Moraxella catarrhalis*, and *Bordetella pertussis*, were found as sources of the infection (Worrall, 2008; Clark *et al.*, 2014; Kinkad and Long, 2016).

Bronchiolitis is an acute lower respiratory tract disease, most prevalent in children, mainly caused by a viral infection (Dalziel *et al.*, 2022). The most common viral agent responsible for bronchiolitis is the human respiratory syncytial virus (RSV). It is an RNA virus with two antigenic strains: RSV-A and RSV-B, and some studies suggest that the RSV-A strain is accountable for higher morbidity (Kuhdari *et al.*, 2018; Efstathiou *et al.*, 2020). Other viruses that cause acute bronchiolitis are human metapneumovirus, rhinovirus, enteroviruses, influenza and parainfluenza viruses (Bush and Thomson, 2007). These viral infections evoke distal bronchiolar inflammation and obstruction of airways, which culminates in limited airflow and altered exhalation capacity. It leads to hyperextension of the lungs, elevated mucus production, and wheezing (Dalziel *et al.*, 2022). RSV launches the expression of inflammatory cytokines, followed by peribronchial and perivascular infiltration of neutrophils and lymphocytes, which cause an unbalanced response between Th1 and Th2 (Fan *et al.*, 2018; Sebina and Phipps, 2020).

Institute for Health Metrics and Evaluation (2020) claims that lower respiratory tract infections caused approximately 2.5 million deaths in 2019. In 2016, most victims were children 5 years old and younger, accounting for approximately 650 000 deaths, and seniors 70 years old and older, causing more than 1 million dead people (Troeger *et al.*, 2018; Forum of International Respiratory Societies, 2021).

3.1.4 Tuberculosis

Tuberculosis (TB) is an infectious respiratory disease caused by the *Mycobacterium tuberculosis* complex, including *M. tuberculosis, M. canettii, M. africanum, M. microti, M. bovis, M. caprae* and *M.pinnipedii*. However, the most significant is *M. tuberculosis* (Smith *et al.*, 2006; Pai *et al.*, 2016). From a clinical and public health perspective, TB is classified as active or passive tuberculosis. (Pai *et al.*, 2016)

After inhalation of bacteria, pathogens are further translocated to the lower respiratory system. Here, they are encountered by alveolar macrophages, the main target of *M. tuberculosis*. Macrophages interact with bacteria, mediated by receptors such as Toll-like receptors. This leads to phagocytosis of *Mycobacterium tuberculosis* (Jordao and Vieira, 2011; Pai *et al.*, 2016). *M. tuberculosis* then blocks the fusion of the phagosome with the lysosome leading to bacteria survival (Russell, 2011). Afterwards, the infection progress to the lung parenchyma, where it spreads, although the mechanism is not fully elucidated. However, two possible mechanisms are considered: direct infection of epithelial cells by *M. tuberculosis* or transmigration of *M. tuberculosis*-infected macrophages across the epithelium. Subsequently, the dendritic cells and inflammatory monocytes are recruited from the bloodstream, transporting pathogens to pulmonary lymph nodes for T lymphocyte priming. T cells and B cells are then transported back to the lung parenchyma to form the granuloma, which separates the infection from the rest of the body (Jordao and Vieira, 2011; Pai *et al.*, 2016). In most infected people, the granuloma contains the infection without triggering tissue pathology resulting in passive TB. However, when the bacterial load is overcome, and the balance is broken, after some time (from weeks to decades), the passive TB can progress to active TB, invading other organs. Three possible mechanisms may lead to the progression from passive to active TB: human immunodeficiency virus (HIV), TNF-neutralizing antibodies and inborn errors in immunity (Jordao and Vieira, 2011; Lin *et al.*, 2013; Pai *et al.*, 2016).

World Health Organization (2022) claims that 10.6 million people developed TB in 2021, and 1.6 million died from it, accounting for 15% of TB patients. Among the patients, 187 000 were co-infected with HIV, approximately 12% of the cases.

3.1.5 Lung cancer

Lung cancer is a heterogeneous disease with broad clinicopathological manifestation. According to World Health Organization (2020), it belongs in the top three most diagnosed cancers among males and females and is a significant cause of mortality (Travis *et al.*, 215).

Lung cancer development is accompanied by multiple genetic and epigenetic alternations that lead to the activation of oncogenes or inhibition of tumour suppressor genes (Larsen and Minna, 2011). The main risk factors for lung cancer are tobacco smoking, exposure to second-hand smoke, environmental air pollution, asbestos inhalation, family history, radon gas exposure and diet. (Malhotra *et al.*, 2016). Two main histotypes of lung cancer may be distinguished into non-small-cell lung cancer (NSCLC) and small-cell lung cancer (SCLC; Thai *et al.*, 2021).

The NSCLC group represents 85% of lung cancer cases, and it includes the following subtypes: adenocarcinoma, which is formed in more distal airways (40%), squamous cell carcinoma arising in more proximal airways (30%) and large cell carcinomas (15%; Chen *et al.*, 2014; Schabath and Cote, 2019). The most prevalent mutations in oncogenes that occur in adenocarcinomas are serine/threonine-protein kinase B-Raf (BRAF), Kirsten rat sarcoma viral oncogene homolog (KRAS), epidermal growth factor receptor (EGFR), human epidermal growth factor receptor 2 (HER2), ROS proto-oncogene 1, receptor tyrosine kinase (ROS1), anaplastic lymphoma kinase (ALK), fibroblast growth factor receptor 1 (FGFR1) and FGFR2, in addition to mutations in tumour suppressor genes, TP53 and RB1, which can be found in all histotypes of lung cancer. In squamous cell carcinoma, the frequently mutated genes are discoidin domain receptor tyrosine kinase 2 (DDR2), FGFR1, FGFR2, FGFR3 and genes in the phosphoinositide-3-kinase (PI3K) pathway (Chen *et al.*, 2014).

In SCLC, which represents 15% of lung cancer cases, the major alternations are associated with RB family genes, phosphatase and tensin homolog (PTEN), NOTCH receptors, cyclic adenosine monophosphate response element binding protein (CREBBP), MYC family genes, FGFR1, guanine nucleotide-binding protein, and alpha stimulating activity polypeptide (GNAS; Rudin *et al.*, 2021).

Lung cancer was the second most prevalent cancer in 2020 after breast cancer, with 2.21 million cases. In 2020, it was the deadliest cancer, with 1.8 million of caused deaths, where 66% of deaths accounted for males and 34% for women (World Health Organization, 2022a; WCRF International, 2022). Incidence was higher in males than females, with approximately 1.44 million diagnosed.

3.2 Lung models in research

In recent years, respiratory diseases have represented a global socioeconomic burden and are the leading cause of morbidity and mortality (Niemeyer *et al.*, 2018; Wisnivesky and de-Torres, 2019). The situation culminated during the COVID-19 pandemic, which clearly

showed the importance of the drug development process and the need for reliable and cost-effective models for respiratory disease research (Lehr *et al.*, 2021). The current drug development model is inefficient because development costs are too high, and the number of new drugs is low. Furthermore, approximately 29% of new medicaments for respiratory diseases fail to transit from phase II to III of clinical trials, which is lower than average for all disease indications (Thomas *et al.*, 2016; Hynes *et al.*, 2020). The critical reason for poor results in clinical trials is the inconsistency of therapeutic candidates identified from preclinical animal testing, possibly due to anatomical, physiological and pathophysiological differences between human and animal lungs (Cidem *et al.*, 2020; Lehr *et al.*, 2021). There are efforts to use improved in vitro lung models relevant to human physiology as an alternative to *in vivo* animal models (Bonniaud *et al.*, 2018).

The following chapters describe models used in respiratory diseases and lung research.
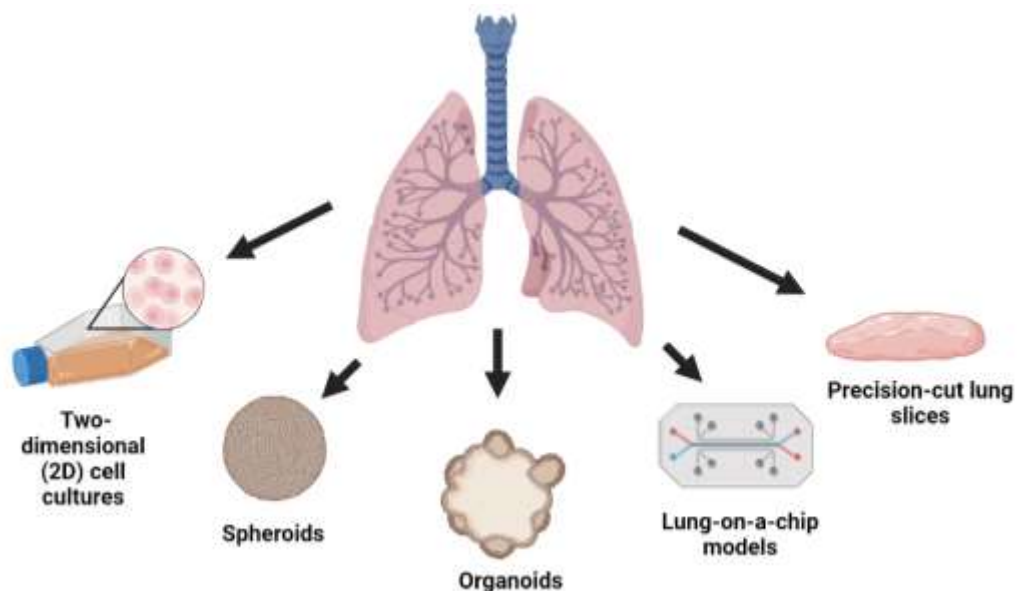
Figure 3. 1: Overview of lung models used in respiratory diseases and lung research (Image was created in BioRender.com)

3.2.1 Two-dimensional (2D) cell culture models

2D cell culture is a widely utilized research tool, which plays an essential role in many research areas, such as cancer research or drug discovery, because cells can be easily exposed to different stimuli or manipulated by various techniques (Kapałczyńska *et al.*, 2016; Hiemstra, 2019).

Adherent 2D cell cultures are grown as monolayers attached to plastic surfaces in culture flasks or Petri dishes, entirely covered by medium, whereas suspension cell cultures have cells floating in the culture medium. Although two main advantages of 2D cell cultures are easier manipulation and low-cost maintenance, certain disadvantages make this system physiologically irrelevant (Breslin and O'Driscoll, 2013; Kapałczyńska *et al.*, 2016). These disadvantages include a lack of cell-cell and cell-extracellular matrix (ECM) signalling, insufficient cell differentiation, and modified gene expression. These features are addressed in more advanced models, such as three-dimensional (3D) and other complex models, which better mimic *in vivo* environments (Kapałczyńska *et al.*, 2016). Table 3.1 provides an extended list of comparisons between 2D and 3D cultures.

2D cell cultures can be established from isolated tissues, known as primary cultures, or provided by bioresource centres such as the American Type Culture Collection (ATCC), which offers immortalized cell lines with higher replicative potential, also known as non-primary cultures (Kapałczyńska *et al.*, 2016; Hiemstra *et al.*, 2018). Immortalized cell lines widely used in lung research are 16HBE, A549, H441, Calu-3 and NHBE. Additionally, human bronchial epithelial cells (HBEC), induced pluripotent stem cells (iPSC) derived epithelial cells and alveolar epithelial cells (AEC) are employed as primary cell lines (Zscheppang *et al.*, 2017; Nikolic *et al.*, 2018; Jensen and Teng, 2020). Immortalized cell lines are advantageous due to the ease of manipulation; however, the ability or potential inability to differentiate *in vitro* must be considered. On the other hand, primary cell lines are directly isolated from human lungs via biopsy or bronchoscopy and are more likely to mimic physiological function than non-primary cell lines. However, their life span is shortened compared to immortalized cell lines, and they are difficult to obtain due to ethical approval or collaboration with hospitals (Hiemstra *et al.*, 2018).

The inefficiency of 2D cell cultures to properly differentiate when submerged in a culture medium indicates the limitations of 2D cell models as complex research models. However, primary cells cultures can be successfully differentiated into 3D polarized mucociliary differentiated airway epithelial layers that accurately reflect the organization and gene expression of airway epithelium in situ, using an air-liquid interface (ALI) technique (Pezzulo *et al.*, 2011; Dvorak *et al.*, 2011; Cao *et al.*, 2015). The ALI technique works by placing the basal surface of the primary cells, such as HBEC, in contact with the medium while the apical side of the epithelial cells is exposed to air. This leads to the proper differentiation of the cells, which then take on features of *in vivo* tissue, including mucus production and apical

cilia generation (Hynes *et al.*, 2020). This technique has been widely used in cystic fibrosis research (Miller and Spence, 2017).

Table 3. 1: Comparison of essential features between 2D and 3D cell cultures (According to Kapałczyńska *et al.*, 2016; Habanjar *et al.*, 2021).

Characteristic	2D	3D
Support for cell adherence	Non-physiological (plastic/polycarbonate)	Extracellular matrix *in vitro*
Cell culture quality	High performance, reproducibility, long-term culture, easy to handle, simplicity of culture	Low performance and reproducibility, difficult to handle, cultures more challenging to carry out
***In vivo* limitations**	Do not mimic the natural structure of the tissue or tumour	*In vivo* tissues and organs are in a 3D environment
Cell interactions	Less cell-cell and cell-extracellular environment interactions, no *in the vivo*-like microenvironment and no "niches"	Higher interactions, similar to real-time cell-cell and cell-extracellular environment, environmental "niches" are created
Cell differentiation	Moderately and poorly differentiated	Well-differentiated
Cell proliferation	Higher proliferation rate	The gradient of proliferating cells
Treatment sensitivity	Cells more sensitive to treatment	Cells less sensitive to treatment
Viability	Sensitive to cytotoxins	Less sensitive to external factors
Cost	Cheaper, more commercially available tests and the media	More expensive, more time-consuming, fewer commercially available tests

3.2.2 Three-dimensional (3D) cell culture models – spheroids and organoids

Currently, two-dimensional (2D) cell cultures are insufficient to accurately replicate the complexities in tissue or organ, such as microarchitecture and dynamic intracellular interactions that occur *in vivo*. This has led to the developing of three-dimensional (3D) cell culture models, regarded as more stringent and representative models (Zanoni *et al.*, 2016; Niemeyer *et al.*, 2018). Table 3.1 outlines some of the limitations of 2D models, which can be overcome by 3D culiuring techniques such as spheroids and organoids, which more closely stimulate the lungs

in vivo (Sakalem *et al.*, 2021). Most 3D cell cultures are categorised as non-scaffold and scaffold-based (Langhans, 2018).

Non-scaffold 3D cell cultures include spheroids, self-assembling cell aggregates formed in an environment that prevents them from attaching to the surface of the culture dish/flask. Examples of such systems include hanging drop microplates (cells suspended due to superficial tension), low adhesion plates with ultra-low attachment coating (for example, agarose or poly-HEMA), and micropatterned plates that allow for microfluidic cell culture. Spheroids can also be produced using the magnetic levitation technique, wherein cells are coupled with magnetic nanoparticles and assembled using a magnetic field. The formation of spheroids is made possible by membrane proteins or extracellular matrix (ECM) proteins secreted by the cells (Langhans, 2018; Białkowska *et al.*, 2020; Sakalem *et al.*, 2021). The clustering of the cells offers a distinct advantage in simulating cell-cell and cell-ECM interaction, making them ideal for modelling malignancies, such as non-small-lung cancer, due to their resemblance to the complexities of tumours, including proliferating and quiescent zones, and regions of hypoxia. Despite these advantages, there are still several issues, such as uniform size, which is controlled by the number of cells seeded or the ratio of cells in co-cultures. (Das *et al.*, 2015; Niemeyer *et al.*, 2018).

Gkatzis *et al.* (2018) describe organoids as self-organized cell aggregates of multiple cell types grown in gels of different ECM proteins, including laminin, fibronectin, and collagen. Organoids are highly similar to actual organs and are generated from pluripotent stem cells (PSCs), such as embryonic or induced PSCs, or adult stem cells (ASCs), by mimicking regeneration and development *in vitro* of multiple organs, such as the intestine, liver and lung. (Fang and Eglen, 2017; Kim *et al.*, 2020; Sakalem *et al.*, 2021). Organoids can exercise the primordial functions of the corresponding organ and are more complex than spheroids. PSCs can be differentiated into organoids through germ-layer specification into endoderm, mesoderm, or ectoderm. Subsequently, the induction and maturation of these cells can be achieved by culturing them with specific growth and signalling factors, allowing for the generation of specific cell types of the desired organ. On the contrary, the derivation of organoid cultures from ASCs necessitates the isolation of the tissue-specific stem cell population, which can then be embedded into an extracellular matrix containing a precisely tailored combination of growth factors to enable its propagation (Kim *et al.*, 2020; Hofer and Lutolf, 2021).

Although spheroids and organoids can be valuable tools for modelling lung physiology and pathophysiology, there are still limitations to be addressed. This has led to more complex

models, such as precision-cut lung slices and organs-on-chips, which offer a more comprehensive approach to understanding lung biology (Niemeyer *et al.*, 2018).

3.2.3 Lung-on-a-chip models

Due to the inability of organoids to replicate complex geometric and mechanical characteristics of organs, more advanced models are needed to more accurately replicate the *in vivo* architecture, microenvironment, and functions of organs to bridge the gaps in existing models. Fortunately, recent advances in microfabrication techniques have enabled researchers to develop advanced models known as organ-on-a-chip (Francis *et al.*, 2022). These microfluidic devices can mimic the physiological and mechanical parameters which regulate and influence organ or system homeostasis and function in a microfluidic cell culture chip (Fang and Eglen, 2017; Nikolic *et al.*, 2018, Cidem *et al.*, 2020). The chips are created precisely using microfabrication techniques such as soft lithography, photolithography and 3D bioprinting (Fang and Eglen, 2017; Agraval and Chu, 2022). Organs-on-chip were developed for several organs, including the liver, kidney, and lungs. (Moreira *et al.*, 2021).

Lung-on-a-chip (LOC) is an advanced multi-layered microfluidic device that accurately replicates the architecture and cellular environment of lungs, thereby reproducing critical physiological functions and responses of lungs *in vivo*. Different types of LOCs have been developed to meet the specific needs of various studies and to study different physiological processes (Francis *et al.*, 2022). Huh *et al.* (2010) were the first to develop a LOC model containing two parallel microchannels separated by a polydimethylsiloxane (PDMS) membrane, which is thin, flexible and permeable. The PDMS membrane is coated with ECM proteins to mimic the alveolar-capillary barrier and is populated with human alveolar epithelial cells on the top side and human pulmonary endothelial cells on the bottom sides. After seeding the cells, the top microchannel is aspirated by air, while the bottom microchannel is infused with the medium. The vacuum is then applied to two lateral channels of the device, stretching the alveolar-capillary interface to stimulate breathing. Zhang *et al.* (2018) investigated the pulmonary toxicity of nanoparticles using a modified model. Their LOC model consisted of three parallel microchannels, with a layer of Matrigel® membrane situated between human alveolar epithelial cells and human vascular epithelium in the central channel to stimulate the alveolar-capillary interface. They added cell-ECM interaction to monitor changes in the barrier integrity after exposure to different concentrations of zinc oxide (ZnO) and titanium dioxide (TiO_2) nanoparticles. Benam *et al.* (2015) designed a human small-airways-on-a-chip to model

COPD and asthma and tested drugs by perfusing IL-13 into lower endothelium microchannel, which led to the hypersecretion of inflammatory cytokines, hyperplasia of goblet cells and other pathological signs of asthma. Upon adding the anti-inflammatory drug tofacitinib, these changes were successfully suppressed. Additionally, the researchers utilized primary airway cells derived from COPD patients to model COPD.

Although LOCs have numerous benefits, there are still significant limitations due to the technical incapability of replicating the entire human complexity and the lack of a standard protocol (Francis *et al.*, 2022).

3.2.4 Precision-cut lung slices

Despite having 2D, 3D and lungs-on-a-chip models to study lungs, researchers can still not accurately replicate the lungs' intricate spatial complexity and cellular richness (Liu *et al.*, 2018). The low availability of human lung tissue, high expenses associated with maintaining animal facilities, and the need to incorporate the 3Rs (Refinement, Reduction, Replacement) principles to reduce the usage of animals have contributed to the development and increased use of precision-cut lung slices, according to Viana *et al.* (2021).

Precision-cut lung slices (PCLS) are small and uniform slices from lung tissue, which retain most of the lung cell types, complex microarchitecture, anatomical structure, and responses to stimuli that are similar to those of native lungs, as well as other lung-specific features (Viana *et al.*, 2021; Agraval and Chu, 2022). PCLS can be obtained from genetically modified or diseased animals, including mice, guinea pigs, sheep and pigs, and human surgical samples, which makes them ideal for bridging the gap between cell models and animal or human subjects (Bryson *et al.*, 2020; Li *et al.*, 2020). PCLS can be utilized for high-resolution live imaging, monitoring of ultrastructural changes, and tracking of cell activity, migration, infection progression, and drug treatments. Fluorescent microscopy helps in observing various markers for different cell types, signalling molecules, and labelled pathogens. Additionally, the culture medium in which PCLS are cultivated can collect and analyse diverse molecules such as metabolites and cytokines. Furthermore, PCLS are widely employed for histological, metabolomic, proteomic, transcriptomic, and immunohistochemical analysis (Viana *et al.*, 2021; Agraval and Chu, 2022). PCLS are used as an *ex vivo* system for toxicology, immunology, pharmacology and alvelogenesis studies of the respiratory system (Akram *et al.*, 2019; Preuß *et al.*, 2022). This is due to the morphologically relevant tissue structure, including small airways, respiratory parenchyma, structural and immune cells, and connective tissue,

which makes PCLS an ideal model for evaluating asthma, COPD, idiopathic pulmonary fibrosis, allergy and infections (Liu *et al.*, 2018). However, these precision-cut tissue slices can be generated from the lungs and other organ tissues, such as the liver or brain (Alsafadi *et al.*, 2020).

3.2.4.1 Generation and cultivation

For the generation of PCLS, the lobes of the lungs are first slowly and steadily inflated with 0.5–3% equilibrated low melting-point agarose solution via the trachea, which prevents the collapse of the lung airways. The volume of the agarose depends on the size of the lungs and the age of the animal. After inflation, the agarose in the lungs is rapidly solidified by submerging them in an ice-cold buffer, and then the tissue is sliced by a vibrating microtome. Subsequently, the PCLS slices are submerged in culture media supplemented with antibiotics, without or with minimal serum, to prevent cell growth and changes to native cellular diversity. The number of lung slices can vary depending on the size of the lungs; for instance, hundreds of precision-cut slices can be generated from a single small human lung lobe. Lung slices can be cryopreserved for future use, as it has a minimal impact on cell viability, airway contraction, and the vital functions of immune cells (Liu *et al*., 2018). PCLS are cut to a size that varies by approximately 5%, with the most commonly used sizes being 100–500 μm. For consistent PCLS generation, biopsy punches can be employed to reduce the size variability. This ensures that the produced PCLS are of a uniform size, allowing for more accurate and reliable results. Finally, the PLCS are incubated in multi-well plates at 37°C, 5% CO_2 and 95–100% air humidity (Sanderson, 2011; Liu *et al*., 2018; Viana *et al*., 2021).

Typically, PCLS are cultured for one week, disadvantaging long-term experiments such as disease modelling (Preuß *et al.*, 2022). However, some studies have discovered that PCLS generated from human lungs can surpass the one-week limit. The viability, structural integrity and metabolic activity were preserved for up to 15 days of cultivation, and PCLS contained all the relevant cell types (Temann *et al*., 2016; Khan *et al*., 2020). Bailey *et al*. (2020) managed to prolong the cultivation of lung slices even up to 3 weeks by using special synthetic PEG-hydrogels for embedding the lung slices, which provided a specific microenvironment for cells. Over the course of long-term cultivation, numerous changes can be observed in lung slices, such as decreased cytokine and chemokine levels after stimulation or persistent inflammation monitored during the first four days of cultivation (Preuß *et al*., 2022).

3.2.4.2 Advantages and disadvantages

The main advantage offered by PCLS is the ability to study the structure and function of the lungs in their natural environment. This technology can be used to conduct paired analyses of multiple treatments in a single patient, investigate the mechanisms of lung-related diseases (as outlined in Chapter 3.3.2), and facilitate drug discovery and toxicological studies (see Chapter 3.3.1) to predict treatment or toxicant effects (Alsafadi *et al*., 2020).

On the other side, a significant drawback of this model is the heterogeneity of the slices, which reflects the current state of the cell populations in the lungs, making data interpretation more difficult. Additionally, drug administration can be challenging, as the whole slice is treated with compounds, making it difficult to translate treatment to inhaled or systematic application *in vivo* (Liu *et al.*, 2018). Furthermore, the inability to mimic ventilation, mechanical stretch or perfusion is considered a limitation.

Despite these disadvantages, PCLS is still a successful model in toxicological, metabolic, and physiological research (Cidem *et al.*, 2020).
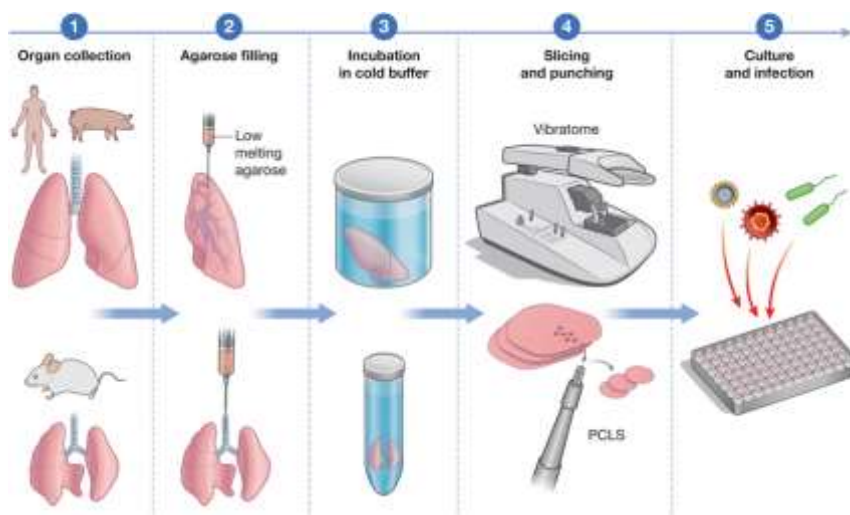
Figure 3. 2: Scheme of precision-cut lung slices (PLCS) generation taken from Viana *et al.* (2021).

3.3 The applications of lung models in research

3.3.1 Drug discovery and development

In vitro and *ex vivo* lung models are essential for drug discovery and development, providing accurate predictions of treatment effects in human tissues and minimizing the number of animals required for *in vivo* research, according to mentioned 3Rs principle. More examples

of lung models and their applications in drug discovery can be found in the literature (Viana *et al.*, 2021; Moreira *et al.*, 2021).

2D cell culture models remain widely utilized in preclinical drug discovery and development, particularly for high-throughput toxicity screening of new compounds due to their cost-effectiveness, convenience, and ease of use (Yaqub *et al.*, 2022). As an example, Henz Ryen *et al.* (2020b) were recently investigating the anti-inflammatory properties of bisabolene sesquiterpenes isolated from *Lindera benzoin* in A549 lung carcinoma cells. Additionally, Felgenhauer *et al.* (2020) investigated the antiviral interferons of type I (IFN-α) and type III (IFN-λ) and their inhibitory activities against severe acute respiratory syndrome coronavirus 2 (SARS-CoV-2) in Calu-3 cell line. However, the two-dimensional cell lines used for respiratory target validation in drug testing research have some limitations, as mentioned in Chapter 3.2.1, which impede proper data evaluation regarding drug efficacy (Yaqub *et al.*, 2022).

3D cell cultures, such as spheroids and organoids, are essential for drug discovery and development due to their more complex characteristics than 2D models and compatibility with high-throughput assays (Fang and Eglen, 2017; Yaqub *et al.*, 2022). Spheroids derived from NSCLC cells are often used for screening new anticancer drugs (Rozenberg *et al.*, 2021). Surolia *et al.* (2017) also utilized spheroids to study idiopathic pulmonary fibrosis from nine subjects to evaluate patients' responses to anti-fibrotic drugs. On the other hand, Kim *et al.* (2019) employed normal bronchial organoids and lung cancer-derived organoids from patient-derived cells to monitor drug response to docetaxel, olaparib, erlotinib, and crizotinib. Moreover, Han *et al.* (2021) developed lung organoids from human pluripotent stem cells to establish a high-throughput screening assay for SARS-CoV-2 inhibitors.

Organs-on-a-chip shows great potential in revolutionizing the drug development pipeline. They can replicate the physiological environment and functionality of human organs, including lungs, on a chip, which is highly useful for disease modelling and drug testing (Ma *et al.*, 2021). Benam *et al.* (2015) employed a human lung small airway-on-a-chip to assess the effectiveness of tofacitinib, a potent pan-inhibitor of Janus kinase-1 (JAK1), -2, and -3, in counteracting the effects of IL13-induced asthma in vitro. Huh *et al.* (2012) investigated drug toxicity-induced pulmonary oedema in human cancer patients treated with interleukin-2 (IL-2) using a lung-on-a-chip model. They discovered a potential new therapeutic, GSK2193874, developed by GlaxoSmithKline, to inhibit transient receptor potential cation channel subfamily V member-4 (TRPV4).

A large number of novel therapies fail in clinical trials; thus, there is an urgent need to develop more clinically relevant translational approaches for drug discovery and validation. PCLS is a suitable tool in this area (Alsafadi *et al.*, 2020). Cedilak *et al.* (2019) used PCLS prepared from mice treated with bleomycin as an *in vitro* model to evaluate antifibrotic compounds such as the ALK5 inhibitor SB525334 and nintedanib. Danov *et al.* (2018) sought to create targeted therapies for severe asthma, such as inhibiting the soluble IL-13 or its receptor IL-4Rα subunit in PCLS, by utilizing four distinct inhibitors. Geiger *et al.* (2022) used aspirin with acetylsalicylic acid as an active compound with antiviral activity against influenza viruses and rhinoviruses to test its usage in inhibiting SARS-CoV-2. They used PCLS generated from human lungs, and the results show a decrease in viral replication by two orders of magnitude. Zimniak *et al.* (2021) investigated whether existing drugs could be utilized as potent inhibitors of SARS-CoV-2. They tested fluoxetine, which effectively inhibited the virus and decreased the infectivity of SARS-CoV-2 in precision-cut human lung slices. Fluoxetine is a racemate, and it was demonstrated that the R-form could be used to treat SARS-CoV-2 in patients belonging to risk groups who have been infected. Delivery of nanoparticles of oligonucleotides offers a promising approach to cancer treatment. In 2011, Dong *et al.* conducted a study using isolated human tumour tissue slices and primary lung cancer cells from NSCLC patients to evaluate the efficacy of chitosan-coated poly(lactide-co-glycolide) nanoparticles as a carrier system. These nanoparticles were used to form complexes with antisense 2-O-methyl-RNA, which binds to the RNA component of telomerase and can effectively inhibit it. Results showed that telomerase activity was inhibited in 50% of tissue slices, the antisense 2-O-methyl-RNA was increased and in 40% of tissue slices. Another cancer research was conducted on NSC 710305, also known as Phortres, a metabolically activated anticancer prodrug that induces the formation of DNA adducts, resulting in hepatotoxicity, bone marrow toxicity, and pulmonary toxicity. Behrsing *et al.* (2012) utilized the PCLS model to investigate the concentration-dependent effects of Phortres on the content of proteins and cytokines and immune and histological endpoints. From their findings, they determined that relevant tissue damage occurred within a few days of administering NSC 710305.

3.3.2 Disease modelling

In medical research, there is a pressing need for human-based disease models to study numerous lung diseases (Zscheppang *et al.*, 2017). *In vitro* and *ex vivo* lung models have become increasingly popular in respiratory research, with disease modelling being one of the

most widely used applications (Moreira *et al*., 2021). Below are some lung models used in disease modelling in recent research.

For decades, 2D human cell lines have been a powerful and basic tool for studying the biology and pathophysiology of the lungs. Despite their limitations, 2D cultures are still widely used in cystic fibrosis research (Miller and Spence, 2017; Barron *et al.*, 2021). Bellec *et al*. (2015) developed CFTR-inactivated human alveolar epithelial cells and Calu-3 cell lines using CRISPR-Cas 9, enabling the manipulation of CFTR expression. Gras *et al*. (2017) employed HBECs from both control and severe asthma patients as ALI cultures to investigate epithelial-dendritic crosstalk in normal and diseased conditions.

Spheroids and organoids have a wide range of applications, from drug discovery to disease modelling, which is enabled by their advantages over 2D models (Table 3.1; Niemeyer *et al*., 2018; Griffin *et al*., 2022). Amann *et al*. (2014) developed 3D spheroid co-cultures of NSCLC cell lines and lung fibroblasts to investigate tumour-stroma interactions. Na *et al*. (2022) wanted to understand the mechanism of SCLC metastasis and thus developed SCLC mouse models with transplanted genome-edited lung organoids, followed by multi-omics analysis. In 2021, Iakobachvili *et al*. studied human airway organoids as models to assess the early steps of mycobacterial infection. They discovered that adult stem cell-derived airway organoids can effectively resolve the early stages of mycobacterial infection.

Lung-on-a-chip models are suitable for predicting complex physiological and pathophysiological processes. Numerous lung-on-a-chip systems have been constructed to simulate various lung physiological and pathophysiological characteristics (Gkatzis *et al.*, 2018). For example, Thacker *et al*. (2020) developed a murine lung-on-a-chip infection model to image the dynamic interactions between host and *Mycobacterium tuberculosis* at an air-liquid interface and to investigate the role of pulmonary surfactant in early infection. Similarly, Zhang *et al*. (2020) created a biomimetic human disease model on a chip to elucidate immune responses and lung injury caused by SARS-CoV-2.

Next to the lung-on-a-chip models, there are PCLSs, which enable improved monitoring of lung pathophysiology by avoiding the limitations of 2D cultures, organoids, and spheroids (Niemeyer *et al*., 2018). Närhi *et al*. (2018) used murine precision-cut slices from Kras-driven non-small-cell lung cancer to show the spatial characteristics of oncogenic signalling and therapy response, which can be further utilized in selecting drug combinations for non-small-cell cancer therapy. Nowadays, e-cigarettes are under intense scrutiny by regulatory authorities due to increasing reports of e-cigarette- or vaping-associated acute lung injuries and their potential toxicity. Moreover, Van Dijk *et al*. (2017) studied the relationship between

parenchyma, airway functionality, and lung repair processes in a COPD model generated from murine PCLSs, and concluded that PCLSs are an appropriate model for certain aspects of COPD pathophysiology. As the SARS-CoV-2 pandemic has paralyzed the world since 2020, research groups have directed their attention to finding an appropriate model to study it. Gerhards *et al*. (2021) conducted a study using precision-cut lung slices (PCLS) obtained from pigs, hamsters, and cats. They observed efficient virus replication in the PCLS of both hamsters and cats. Their results suggest that PCLS may be an effective model for screening sensitivity to newly emerged viruses of different animal species, providing invaluable insight into the spread of the virus. In 2023, Herbert *et al*. conducted a study using mouse PCLS to investigate the impact of condensates prepared from the aerosolized vehicle, nicotine, nicotine with menthol, and e-fluids from e-cigarettes on PCLS. Their findings concluded that these condensates induced pulmonary toxicity and impaired essential physiological functions in the lung, thus confirming the concerns surrounding e-cigarettes. Rosales Gerpe *et al*. (2018) employed a procedure for generating precision-cut slices from sheep and murine tissue from regular and murine melanoma tumour-bearing lungs. They elucidated that PCLS have many applications, such as characterizing the tissue tropism of viruses, assessing the transducing properties of gene therapy vectors, or exploring the tumour specificity of oncolytic viruses.

4 MATERIALS AND METHODS

4.1 Biological material

- BALB/c mice, ranging from 8 to 20 weeks old, were used for the following experiments provided by the Animal facility of the Institute of Molecular and Translational Medicine (IMTM) in Olomouc.

4.2 Chemicals and solutions

Chemicals

- 10x Tris/Glycine/SDS (Bio-Rad, #1610772)
- 2-Mercaptoethanol (Sigma-Aldrich, #125K0165)
- 30% Acrylamide/Bis-acrylamide 29:1 (Bio-Rad, #1610156)
- Amphotericin B (Sigma-Aldrich, #A9528)
- Bovine Serum Albumin (Sigma-Aldrich, #A7906-100G)
- Calcein Blue, AM (Thermo Fisher Scientific, #C1429)
- cOmplete™ Protease Inhibitor Cocktail (Roche, #04693116001)
- Dexamethasone (Sigma-Aldrich, #D4902-1G)
- Dimethyl sulfoxide (Serva, #67-68-5)
- Dulbecco's Modified Eagle Medium (Lonza, #12-604F)
- Dulbecco's Modified Eagle Medium:F12 (Lonza, #BE12-719F)
- eBioscience™ Cell Stimulation Cocktail (500X) (Thermo Fisher Scientific, #00-4970-93)
- Ethanol absolute (Penta Chemicals Unlimited, #71380-11001)
- Formaldehyde solution 35% (Fagron, #614147)
- Gentamicin (Diagnovum, #D904-100ML)
- Hoechst-33342 nuclear dye (Invitrogen, #H21492)
- jetPRIME® buffer (Polyplus, #712-60)
- jetPRIME® polyplus transfection kit (Polyplus, #114-15)
- MTS assay kit (Abcam, #ab197010)
- Opti-MEM™ I Reduced-Serum Medium (Thermo Fisher Scientific, #11058021)
- PhosSTOP™ EASYpack (Roche, #04906837001)

- Pierce™ Bovine Serum Albumin Standard Pre-Diluted Set (Thermo Fisher Scientific, #23208)

- Polybrene Infection/Transfection Reagent (Sigma-Aldrich, #TR-1003-G)

- Propidium Iodide (Sigma-Aldrich, #537059)

- Protease Inhibitor Cocktail Tablets (Roche, #9005-64-5)

- Resolving gel buffer 1.5 M Tris-HCl pH 8.8 (Bio-Rad, #161-0798)

- RIPA Lysis and Extraction Buffer (Thermo Fisher Scientific, #89901)

- Spectra™ Multicolor Broad Range Protein Ladder (Thermo Fisher Scientific, #26634)

- Stacking gel buffer 0.5 M Tris-HCl pH 6.8 (Bio-Rad, #161-0799)

- Tetramethylethylenediamine (Bio-Rad, #1610801)

- Trans-Blot Turbo 5x Transfer Buffer (Bio-rad, #10026938)

- Triton™ X-100 (Sigma-Aldrich, #9036-19-5)

- TWEEN® 20 (Sigma-Aldrich, #1610799)

- Visikol® HISTO-M (Visicol, #HM-100)

- Xylene mixture of isomers (VWR Chemicals, #28975.291)

Solutions

- 1% stock solution of eosin: 1g of eosin dissolved in 20 ml of dH20 and added 80 ml of 96% ethanol.

- 1× TBST buffer: 100 ml of 10× TBS buffer, 0.1% of Tween 20 and added dH2O to 1000 ml.

- 10% (w/v) SDS.

- 10% hematoxylin stock solution in 96% ethanol: 1 g hematoxylin dissolved in 10 ml of 96% ethanol.

- 10% resolving polyacrylamide gel (10 ml): 3.8 ml of dH2O, 3.4 ml of 30% acrylamide/bis-acrylamide mixed with 2.6 ml of resolving gel buffer and added 100 μl of 10% (w/v) SDS, 100 μl of 10% (w/v) APS and 10 μl of TEMED.

- 10× PBS: 80 g NaCl, 2 g KCl, 14.4 g Na2HPO4, 2.4 g KH2PO4 dissolved in 800 ml dH2O, pH adjusted to 7.4 with HCl and added dH2O to 1000 ml, sterilized by autoclaving.

- 10× TBS buffer: 24 g Tris base and 88 g NaCl dissolved in 900 ml dH2O, pH adjusted to 7.6 with HCl and added dH2O to 1 000 ml.

- 2% stock solution of H5IO6: 0.5 g of H5IO6 dissolved in 25 ml of dH20.

- 25% ethanol: 25 ml of absolute ethanol mixed with 75 ml of dH2O.

- 3% stock solution of concentrated HCl (35%): 8.6 ml of concentrated HCl (35%) mixed with 100 ml of dH20.

- 3D Fixating Solution: 1.5 g Na_2HPO_4 and 1.13 g NaH_2PO4 dissolved in 27 ml of 35% formaldehyde solution, added 5 ml DMSO and added dH2O to 250 ml.

- 5% (w/v) BSA blocking solution: 2.5 g BSA dissolved in 40 ml of TBST buffer, added TBST to 50 ml.

- 5% stock solution of $KAl(SO4)_2 .12H2O$: 5 g of $KAl(SO4)$ $_2 .12H2O$ dissolved in 100 ml of dH20.

- 5× SDS loading buffer: 250 mM Tris-HCl (pH=6.8), 10% SDS, 30% glycerol, 0.5 M DTT, 0.02% bromophenol blue mixed with 10% beta-mercaptoethanol.

- 50% ethanol: 50 ml of absolute ethanol mixed with 50 ml of dH2O.

- 75% ethanol: 75 ml of absolute ethanol mixed with 25 ml of dH2O.

- 80% glycerol

- Blocking buffer: 5% BSA, 1% goat serum, 1% donkey serum, and 10% DMSO mixed with buffer 1.

- Buffer 1: 50 ml of 10× PBS mixed with 1 ml of Triton-X- and added dH2O to 500 ml.

- Buffer 2: 50 ml of 10× PBS, 1 ml of Tween 20 mixed with 0.5 ml of Heparin and added dH2O to 500 ml.

- Eosin: 30 ml of 1% stock solution of eosin, 60 ml of 80% ethanol mixed with 450 µl of concentrated CH3COOH.

- HBSS/HEPES buffer: 0.14 g $CaCl_2$, 0.1 g $MgCl_2.6H_2O$, 0.1 g $MgSO_4.7H_2O$, 0.4 g KCl, 0.06 g KH_2PO4, 0.35 g $NaHCO_3$, 8 g NaCl, 0.06 g Na_2HPO_4, 1 g Dextrose, 4.76 g Hepes, dissolved in 800 ml dH2O, pH adjusted to 7.4 with HCl and added dH2O to 1000 ml, sterilized by filtering.

- Hematoxylin: 50 ml of 5% stock solution of $KAl(SO4)_2 .12H2O$, 1 ml of 10% hematoxylin stock solution in 96% ethanol mixed with 1 ml of 2% stock solution of H5IO6 and added 10 drops of 3% stock solution of concentrated HCl (35%).

- Permeabilizing buffer: 2.3 g glycine dissolved in 80 ml of buffer 1, added 20 ml of DMSO to 100 ml.

- RIPA buffer (radioimmunoprecipitation assay buffer): 150 mM sodium chloride, 1.0% NP-40, 0.5% sodium deoxycholate, 0.1% SDS (sodium dodecyl sulfate), 50 mM Tris, pH 8.0.

- Stacking polyacrylamide gel (5 ml): 2.975 ml of dH2O, 670 μl of 30% acrylamide/bis-acrylamide, 1.25 ml of stacking gel buffer, 50 μl of 10% (w/v) SDS, 50 μl of 10% (w/v) APS, 5 μl of TEMED.

- Transfer buffer: 200 ml of transfer buffer mixed with 600 ml of dH2O and added 200 ml of ethanol to 1000 ml.

- Washing medium: Dulbecco's Modified Eagle Medium supplemented with 100 nM Dexamethasone, 20 μg/ml Gentamycin, 1.25 μg/ml Amphotericin B and 1× Penicillin/Streptomycin.

4.3 Drugs

- Cyclophosphamide (University Hospital Olomouc)
- Methotrexate (University Hospital Olomouc)

4.4 Antibodies

- Donkey anti-Mouse IgG (H+L) Highly Cross-Adsorbed Secondary Antibody, Alexa Fluor 488 (Thermo Fisher Scientific, #A-21202),1:1000 and 1:2000

- Goat anti-Rabbit IgG (H+L) Highly Cross-Adsorbed Secondary Antibody, Alexa Fluor 488 (Thermo Fisher Scientific, #A-11034), 1:1000 and 1:2000

- Mouse anti-E-Cadherin (4A2) Monoclonal Antibody (Cell Signaling Technology, #14472S), 1:500 and 1:1000

- Rabbit anti-ACE2 Monoclonal Antibody [EPR24705-45] (Abcam, ab272500), 1:50

- Rabbit anti-GAPDH (14C10) Monoclonal Antibody (Cell Signaling Technology, # 2118), 1:4000

4.5 Equipment and software

Equipment

- 24-well Tissue Culture Test Plates (TPP)
- 6-well Tissue Culture Test Plates (TPP)
- Bio TDB-100 Dry block thermostat (Biosan)
- Branson Sonifier® Digital Ultrasonic Cell Disruptor (Branson)
- ChemiDoc MP analysis (BioRad)

- Electrophoresis and Blotting Vertical Apparatus (BioRad)

- Enspire Multimode Plate reader 2300-001M (Perkin Elmer)

- HeracellTM VIOS incubator (ThermoFisher Scientific)

- Leica VT1200 - Semi-Automatic Vibrating Blade Microtome (Leica Biosystems)

- Microdermal Biopsy Puncher biopsy needles, 5.0 mm (Medical)

- Microscope Axio Lab.A1(Zeiss)

- Millicell Cell Culture Insert, 12 mm, polycarbonate, 0.4 µm (Merck Milipore)

- Millicell Cell Culture Insert, 30 mm, hydrophilic PTFE, 0.4 µm (Merck Millipore)

- MSC-Advantage Biological Safety Cabinet (flow-box) (Thermo Fisher Scientific)

- Olympus IX51 Inverted Phase Contrast Fluorescence Microscope (Olympus)

- Rotina 420 R Centrifuge (Hettich)

- SRT9 Rollermixer Lab Roller (Stuart)

- Sterican Needles 0.70 x 30mm, 22-gauge (B. Braun)

- Trans-Blot Turbo Mini 0.2 µm Nitrocellulose Transfer Packs (BioRad)

- Trans-Blot Turbo Transfer Stacks Mini Size (Biorad)

- Trans-Blot Turbo Transfer System (BioRad)

- Ultra Low Temperature Freezer (New Brunswick)

- Vortex V-1 Plus (Biosan)

- Zeiss Spinning Disk Confocal Microscope (Zeiss)

Software

- ImageJ (ver. 1.53q)

- Microsoft Excel

- GraphPad Prism

- Zen 2014 SP1, ver. 9.2 (Zeiss)

4.6 Methods

4.6.1 Precision-cut lung slicing and in vitro culture

Precision-cut lung slices were obtained from BALB/c mice anaesthetized with dimethyl ether and humanely euthanized via cervical dislocation by an animal technician. The anterior chest wall was then excised (Fig. 4.1A), and each lung was filled (needle size 22) with pre-heated 1% low-melting-point agarose dissolved in a medium through the trachea via injection

25

(Fig. 4.1B). The filled lungs were placed in ice-cold $1\times$ HBSS/HEPES buffer to solidify the agarose. Subsequently, the lobes of the lungs were separated with a scalpel and placed in 2% low-melting-point agarose dissolved in HBSS/HEPES buffer (see Fig. 4.1C). Dr Das then used an automated vibratome to cut the lung lobes in 2% low-melting-point agarose into 300 μm sections in an ice-cold HBSS/HEPES buffer (Fig. 4.1D). Slices of similar size were carefully selected, washed with a washing medium, and two to three slices (or punches) were placed into a 6-well plate on 0.4 μm-cell culture inserts. The precision-cut lung slices were incubated in a humidified incubator with 5% CO_2 at 37°C in four different conditions: Dulbecco's modified Eagle's growth medium (DMEM), with or without 1% fetal bovine serum (FBS), and Dulbecco's Modified Eagle Medium/Nutrient Mixture F-12 (DMEM-F12) with or without 1% FBS. Each medium was supplemented with $1\times$ HEPES, 1% Penicillin-Streptomycin, 20 μg/ml Gentamycin, 1.25 μg/ml Amphotericin B, and 4 mM L-glutamine. The media was changed every other day.
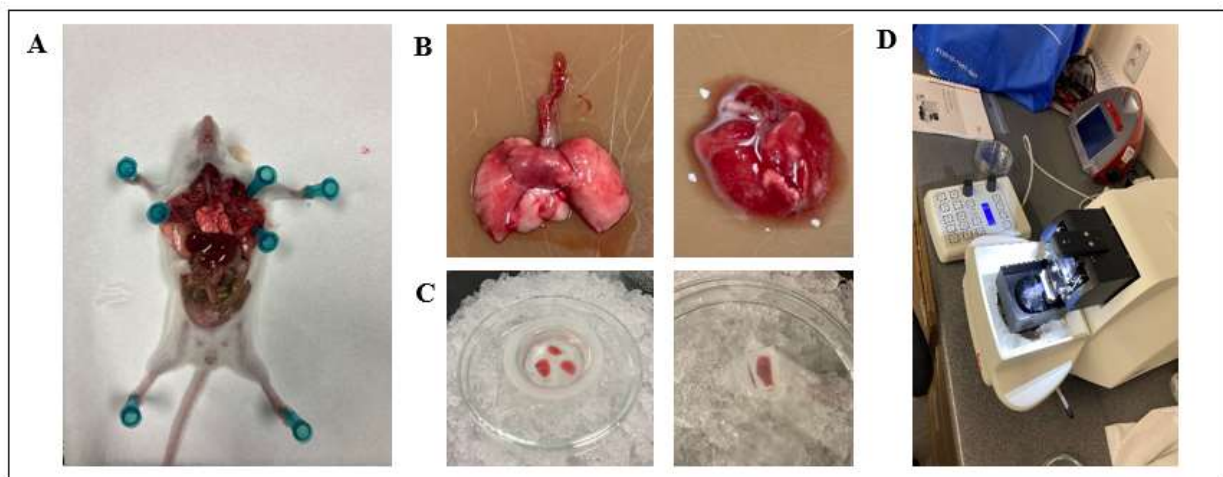
Figure 4. 1: Generation of precision-cut lung slices. (A) The exposed chest cavity of a BALB/c's mouse showing the anterior of the chest wall with unremoved lungs. (B) Removed lungs before (right) and after (left) filling with 1% agarose dissolved in the medium through the trachea using a 22-gauge needle. (C) Separated lung lobes embedded in 2% low-melting-point agarose dissolved in HBSS/HEPES buffer and placed on ice to solidify before cutting. (D) The cutting of the murine precision-cut lung slices using the vibratome.

4.6.2 Viability assay

For determining the viability of PCLS, Propidium Iodide (PI) and Calcein Blue AM (CAM) were used. PI is impermeable in healthy cells with intact membranes, but upon membrane damage, it can enter the cell and bind to double-stranded DNA by intercalating between base pairs. On the other hand, CAM is a cell-permeable derivative of calcein with acetomethoxy groups, giving it a high hydrophobicity and allowing it to penetrate the cell membrane. After the CAM enters the cell, acetomethoxy groups are hydrolyzed by esterases.

Lung slices were collected on day 0 immediately after cutting and on days 1-6 after incubation. The PLCS were incubated with a 2 µM CAM and 2 µg/ml PI mixed with Opti-MEM™ Reduced Serum Medium for 30 minutes at 37°C. Subsequently, they were washed three times with 1× PBS, transferred to a 1.5 ml Eppendorf tube, and fixed with 3D Culture Fixing Solution for 30 minutes at room temperature on a roller. After fixation, the PLCS were again washed three times with 1× PBS. Then, the microscopic slides were prepared by transferring the slices onto microscopic slides, adding 80% glycerol to cover the PLCS, carefully covering them with a cover glass, and imaging them using a confocal microscope with objective 60×. The images were then processed using ImageJ software, and the data were analyzed using Microsoft Excel, Zen 2014 SP1 and GraphPad Prism software.

4.6.3 Histological analysis

PCLS were fixed on day 7 *in vitro* with 3D Culture Fixing Solution for 30 minutes at room temperature on a roller, washed with 1× PBS, followed by staining with hematoxylin and eosin (H&E). Dr Marta Khoylou from IMTM conducted all H&E procedures. PCLS were embedded in parafilm, sectioned into 4 µm thin slices, and placed onto microscopic slides. The slides were then deparaffinized by incubating three times in xylene for 5 minutes, followed by incubation in 100%, 80%, and 70% ethanol for 5 minutes each. The remaining ethanol was washed off with distilled water. The sections were then stained in hematoxylin for 1 minute and washed in distilled water for 3 minutes, followed by 30-second staining in eosin and 1 minute of washing in distilled water. After staining in H&E, the slides were dehydrated for 1 minute in acetone, then in acetone: xylene (1:1) and lastly in xylene for 3 minutes to clarify. The slides were left in a fume hood to evaporate xylene. The slices were then embedded using 10 µl of Peretex and covered with a cover glass.

Stained slice images were captured using a ZEISS Axio Lab A1 microscope with a 10× objective. The images were then processed using ImageJ, and the data were analyzed using Microsoft Excel and GraphPad Prism software.

4.6.4 Transduction of PCLS

PCLS were transduced with 25%, 50%, and 100% transduction mixtures of Arl13b (L13-Arl13bGFP, #40879; Addgene) and 0.25×, 0.5×, and 1× ACE2 lentiviral particles purchased (pWPI-IRES-Puro-Ak-ACE2, #154985-LV; Addgene).

Arl13b lentiviral particles were obtained by seeding 15×10^6 HEK293T/17 cells per 75-cm^2 flask before the transduction. After reaching 80–90% confluency, the HEK 293T/17 cells were transduced with a prepared transfection mixture of plasmid vector in 1.5 ml jetPrime buffer supplemented with 90 μl of jetPrime reagent, following the manufacturer's protocol. The old medium was replaced with 15 ml of fresh growth medium before adding the transfection mixture to the cells. Subsequently, the cells were incubated for 16 hours. After the incubation period, the old medium was replaced with 20 ml of fresh complete-growth medium to allow viral production to continue for 72 hours post-transfection of HEK 293T/17 cells. Cells that were producing viruses had a distinct, rounded phenotype. The medium was collected in a Falcon tube, centrifuged for 5 minutes at 1500 rpm, and filtered through a 0.45-μm filter using a 20 ml syringe.

Afterwards, the old medium from the plates containing PCLS was removed and replaced with the Arl13b lentiviral particle-containing filtered supernatant or ACE2 lentiviral particles. The slices were supplemented with 8 μl/ml polybrene to improve transduction. After 24 hours, the medium was changed to DMEM with 1% FBS, and PCLS were allowed to incubate for 48 hours. Transduced PCLS were fixed with 3D Culture Fixing Solution for 30 minutes at room temperature on a roller, followed by staining with 10 μM Hoeschst 33342 in Buffer 2 overnight at 4°C and continued according to the protocol in Chapter 4.6.6.

4.6.5 Drug treatment and MTS assay

After two days of incubation, the viability of PCLS was assessed using an MTS viability assay. This assay is based on the reduction of the 3-(4,5-dimethylthiazol-2-yl)-5-(3-carboxymethoxyphenyl)-2-(4-sulfophenyl)-2H-tetrazolium (MTS) by viable cells, which

produces a coloured formazan dye that is soluble in cell culture media. The formazan dye is then quantified by measuring the absorbance at 490 nm.

In a 24-well plate, a mixture of 400 µl of DMEM with 1% FBS and 80 µl of MTS was prepared. PCLS punches on 0.4 µm-cell culture inserts were submerged in the solution and incubated for 3 hours in a humidified incubator with 5% CO_2 at 37°C. Then, 100 µl of the mixture was transferred to a 96-well plate, and the absorbance (*Pre-treatment MTS*) was recorded at 490 nm using an Enspire Multimode Plate reader. PCLS were washed in 1× PBS and DMEM with 1% FBS before transferring them into a new 24-well plate cultured containing DMEM with 1% FBS spiked with 5, 25 and 50 µg/ml methotrexate and 10, 150 and 500 µg/ml cyclophosphamide. After four days of treatment, the MTS assay was conducted again, as described above, and the absorbance was recorded as *post-treatment MTS*. In a parallel experiment, PCLS were also treated with the Cell Stimulation Cocktail (0.25×, 0.5×, 1× and 2×) for 24-48 hours. The absorbance data were processed with Microsoft Excel, Zen 2014 SP1 and GraphPad Prism software.

All treated PCLS were collected and processed for immunofluorescence staining and Western blot analysis, as described in Chapters 4.6.6 and 4.6.9, respectively.

4.6.6 Immunofluorescence staining

PCLS were fixed on a roller with a 3D Culture Fixing Solution for two hours. The fixed slices were washed three times with 1× PBS and permeabilized with a permeabilizing buffer overnight at 4°C on the roller. The slices were next blocked in a blocking buffer by gently mixing on a roller at 4°C overnight to prevent the non-specific binding of antibodies. The following day, the PCLS were incubated with primary mouse anti-E-Cadherin (1:500) or primary rabbit anti-ACE2 (1:50) in Buffer 2 supplemented with 5% DMSO, 3% donkey serum and 3% goat serum for 24 hours at 4°C on a roller. After incubation with primary antibodies, the PCLS were washed for 30 minutes three times with Buffer 2. The washed slices were stained overnight on a roller at 4°C with anti-mouse conjugated with Alexa 488 fluorescent dye (E-Cadherin) and anti-rabbit secondary antibodies conjugated with Alexa 488 (ACE2) in Buffer 2 supplemented with 3% donkey serum, 3% goat serum and 5% DMSO. Lastly, the PCLS were stained with 10 µM Hoeschst 33342 in Buffer 2 overnight at 4°C, then washed for 30 minutes three times with Buffer 2.

A clearing protocol was conducted to make the slices transparent and for better imaging of thick PCLS by fluorescent microscopy. Following washing, the PCLS were treated

sequentially with 25%, 50%, 75%, and 96% ice-cold ethanol by gently agitating for 30 minutes on a roller. The ethanol was discarded, and the samples were submerged in Visicol Clearing reagent until imaging (1-24 hours). For imaging, the PCLS were transferred onto slides submerged in Visicol Clearing reagent and covered with a cover glass. They were then imaged using a confocal microscope with 60× objective, and the images were processed using ImageJ software. The data were analyzed using Microsoft Excel, Zen 2014 SP1 and GraphPad Prism software.

4.6.8 Sample processing

After treatment with methotrexate and cyclophosphamide (Chapter 4.6.5), PCLS were collected in 1.5 ml Eppendorf tubes and lysed in 100 µl of RIPA lysis buffer, supplemented with protease and phosphatase inhibitors. The samples were kept on ice throughout the procedure. The samples were snap-frozen on dry ice and thawed on ice, followed by homogenization on a water bath sonicator for 1 minute at 50% Amplitude with a 15-sec pulse ON and 15-sec pulse OFF. After sonication, the samples were agitated on a shaker for 1 hour at 1400 RPM. The homogenized samples were centrifuged at 16 000 RPM at 4 °C for 30 minutes, and the supernatant was transferred to a new pre-cooled 1.5 ml Eppendorf tube. Samples were either processed immediately or stored at –80 °C.

The protein concentration of samples was quantified using a BCA Protein Assay Kit. Bovine serum albumin protein standards (2000, 1500, 1000, 750, 500, 250, 125, 25 and 0 µg/ml) were used to create a calibration curve. The BCA Reagent A and Reagent B were mixed in a 50:1 ratio, and 10 µl of each standard and 1 µl of samples were pipetted into separate wells of a 96-well plate. 200 µl of the BCA reagent mixture was then added to each well. The plate was incubated at 37 °C for 30 minutes, and the absorbance was measured using an EnSpire Multimode Plate Reader at 562 nm. Microsoft Excel generated the calibration curve, and the sample protein concentration was calculated accordingly.

4.6.9 SDS-PAGE Electrophoresis and Western blotting

1.5 mm thick 10% SDS-polyacrylamide gels with 15 wells were prepared. Samples were prepared by adding 35 µg of protein and 4 µl of SDS gel loading dye supplemented with 10% beta-mercaptoethanol and RIPA lysis buffer to bring to the final volume 20 µl per well. This mixture was heated in a dry thermal block at 95°C for 5 minutes. After cooling, the mixtures were loaded onto the gel and electrophoresed at 120 V for 1-1.5 hours.

Electrophoresed samples were transferred onto a 0.2 μm nitrocellulose membrane using a Trans-Blot Turbo Transfer System – Ready-to-Assemble kit using a protocol for 1.5 mm gel with a transfer time of 15 minutes. The nitrocellulose membranes were transferred to 50 ml conical tubes and blocked in 5% BSA in TBS-T solution overnight at 4°C on a roller. The following day, the membranes were incubated on a roller with primary antibodies against E-Cadherin and GAPDH overnight at 4°C. Subsequently, the membranes were washed four times in 1x TBS-T for 10 minutes each. The membranes were next stained with secondary anti-mouse and anti-rabbit antibodies conjugated with Alexa 488 fluorescent dye for 2 hours at 4°C on a roller in the dark. The secondary antibody was removed, and the membranes were washed four times with 1× TBS-T for 10 minutes each and imaged in the Bio-Rad Gel Documentation system. The images were then processed using ImageJ software, and the data were analyzed using Microsoft Excel and GraphPad Prism software.

5 RESULTS

## 5.1 Generation of PCLS and optimization of the culturing

Precision-cut lung slices from mice were obtained using a vibratome. The freshly cut slices were immediately stained and fixed, while others were cultured for six days under four different conditions, as outlined in Chapter 4.6.2. The PCLS fixed in methanol (MeOH) was used as a positive control, and the results are expressed as the percentage MeOH-treated control. The stained slices were imaged using a Zeiss Spinning Disk Confocal Microscope and analyzed using ImageJ.

The number of propidium iodide-positive cells (dead cells) was counted in at least three slices per condition and three focal regions per slice to ascertain the effect of various growth mediums on the long-term survival of PCLS. The number of Calcein AM-positive cells, representing viable cells, was not counted due to the difficulty of precisely localizing them (Figure 5.2). The results (Figure 5.1A) showed that the presence of fetal bovine serum had a significantly positive impact on the viability of the cells in PCLS. Specifically, PCLS cultured in a medium containing 1% FBS had fewer PI-positive cells. The viability of PCLS altered over time, increasing until day 3 and gradually beginning to decline from day 3 (Figures 5.1A and 5.2).

The change in the alveolar area was determined in at least three slices per condition and three focal areas per slice. In the focal area, three alveoli in a z-stack were analyzed. No significant differences or correlations were observed during the six-day study period (Figure 5.1B). The same was true for the change in the alveolar wall thickness (Figure 5.1C), which was measured as the thickness of three walls in a z-stack. At least three slices per condition and three focal areas per slice were analyzed.
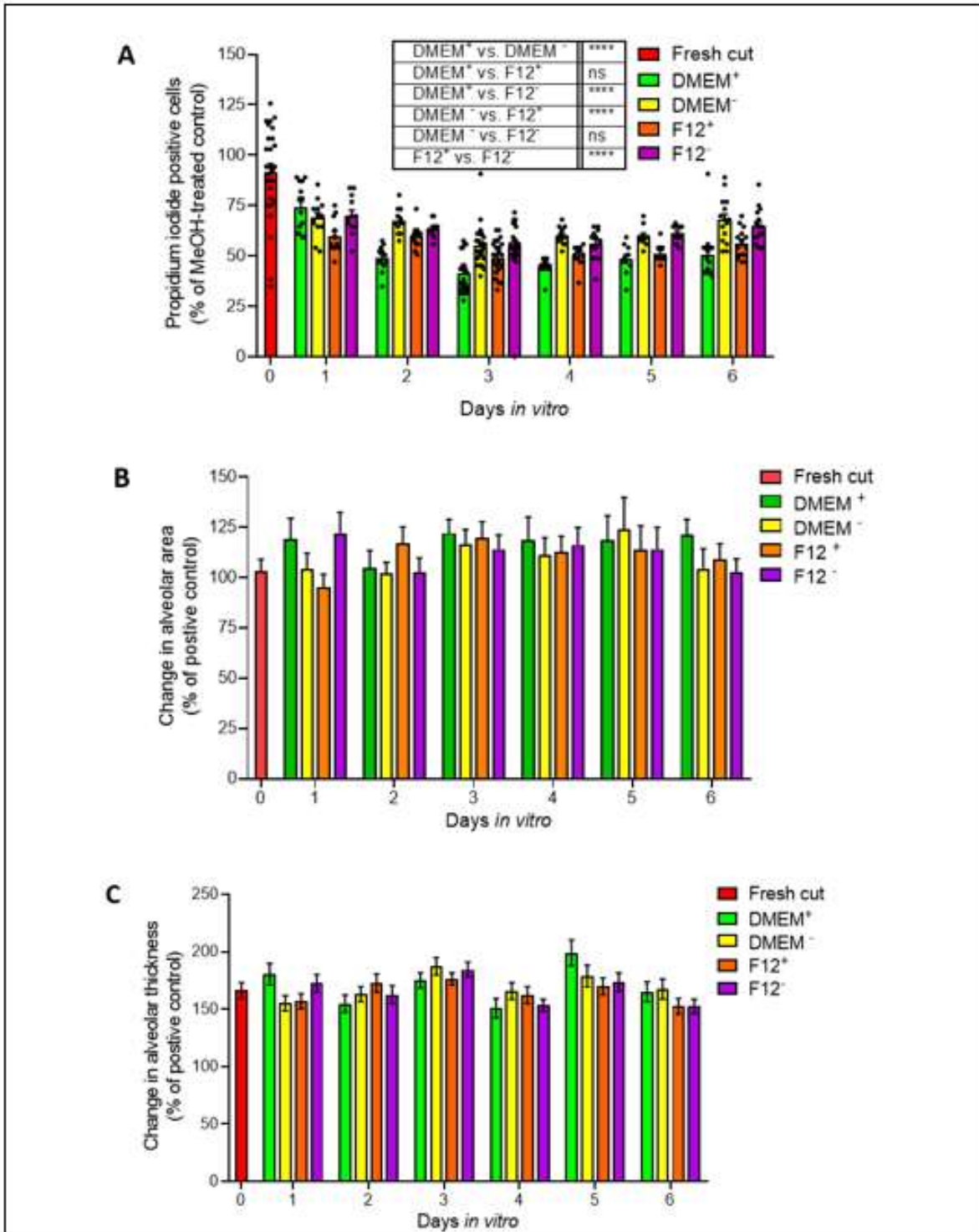
Figure 5. 1: Optimization of PCLS culturing during six days in four conditions. Bar graphs of (A) Propidium iodide positive cells with a table showing statistical differences between conditions (two-way ANOVA, Tukey's multiple comparison test, ****$p < 0.0001$. Statistically insignificance, ns). (B) Change in the alveolar area. (C) Change in alveolar thickness. Data are presented as mean ± SEM, n = 5 separate mice.
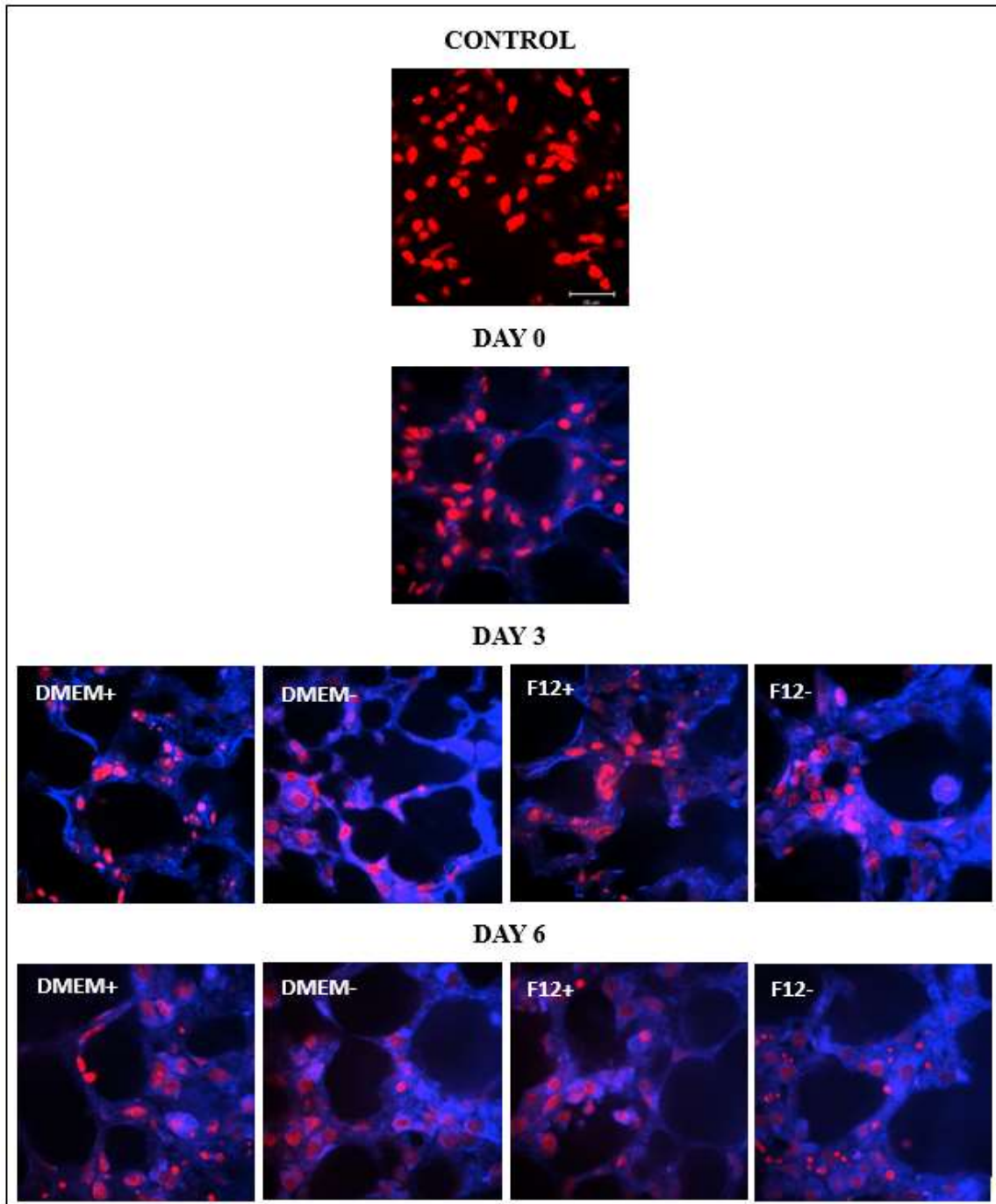
Figure 5. 2: Images of PCLS stained with propidium iodide and Calcein AM. Positive control was treated with methanol. Day 0 indicates freshly cut PCLS without culturing in any media. Day 3 and Day 6 indicate PCLS cultured for 3-6 days in DMEM+, DMEM-, F12+ and F12-. All slices were fixed in formalin, except methanol-treated slices, and stained with propidium iodide (red) and Calcein AM (blue). Objective 60×, Scale bar 20 μm, n = 5 separate mice.

5.1.1 Histological analysis of PCLS

Further, histological analysis confirmed the best condition for culturing the lung slices. The PCLS were cultivated for 7 days, after which histological staining with haematoxylin and eosin was conducted, as stated in Chapter 4.6.3, to assess their condition under four culture different conditions.

The number of alveoli was counted from 3 focal areas per slice, and at least 3 slices per condition were analyzed. The results show that the number of alveoli was highest in PCLS cultured in DMEM+ (Figures 5.3A and 5.4). Conversely, the lowest number was observed in PCLS cultured in F12- ($p < 0.0001$, one-way ANOVA).

Another characteristic measured was noted in the alveolar area per 10 000 μm^2. There were significant differences among the different conditions ($p < 0.0001$, one-way ANOVA). Figures 5.3B and 5.4 show that a larger alveolar area was observed in DMEM- and F12+, respectively, while the smallest alveolar area was noted under F12- growth condition.

Alveolar wall thickness was also determined in at least 3 slices per condition and 3 focal areas per slice. The alveolar wall thickness of 3 walls was measured in a z-stack. The results (Figures 5.3C and 5.4) reflect that alveolar wall thickness was less influenced by the media used for culturing ($p = 0.0245$, one-way ANOVA).

The mean linear intercept (Lm) was used to establish the morphometric changes in lung tissue, determined by serial measurements of the lung using test lines (Crowley *et al*., 2019). Lm analysis was conducted according to Akram *et al*. (2019). At least 3 slices per condition and 3 focal areas per slice were imaged. Within each focal area, Lm was measured using three random squares with a size of 100 μm^2. As observed from Figure 5.3D, the Lm value was lower in DMEM media than in F12 and decreased further when FBS was present ($p < 0.0001$, one-way ANOVA). A smaller Lm indicates a higher density of septa and more alveoli (Akram *et al.*, 2019), which correlates with results from the graph shown in Figure 5.3A.

It was concluded that day 3 and DMEM+ medium were the best conditions for the remaining experiments with PCLS.
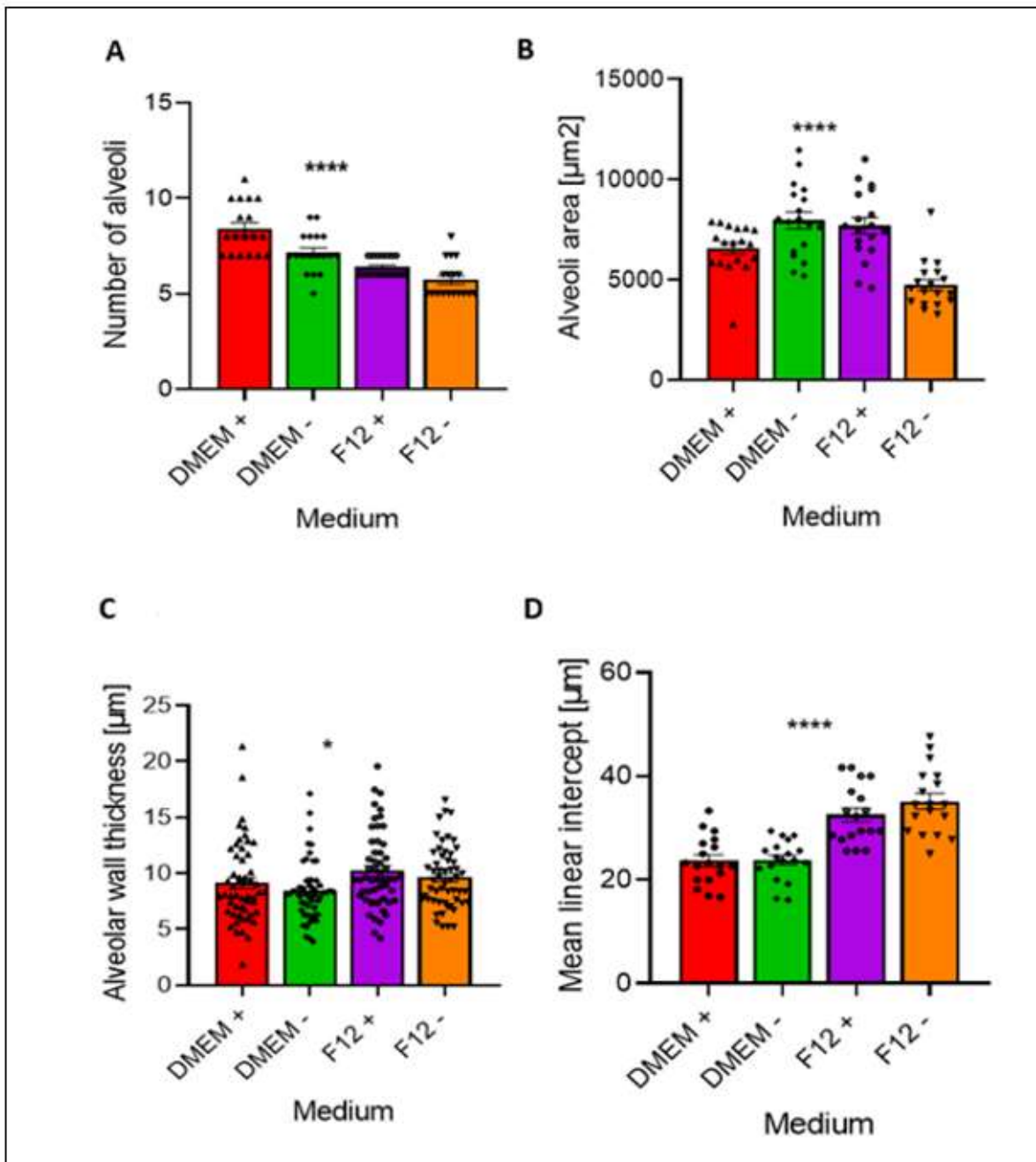
Figure 5. 3: Histological analysis of PCLS in four different conditions after 7 days of culturing by haematoxylin and eosin staining. (A) Quantification of alveoli per 10 000 μm^2 (****$p < 0.0001$, one-way ANOVA). (B) Alveolar area per 10 000 μm^2 (****$p < 0.0001$, one-way ANOVA). (C) Alveolar wall thickness per 10 000 μm^2 (****$p = 0.0245$, one-way ANOVA). (D) Mean linear intercept (****$p < 0.0001$, one-way ANOVA). Data are presented as mean $\pm$ SEM, n = 2 separate mice.
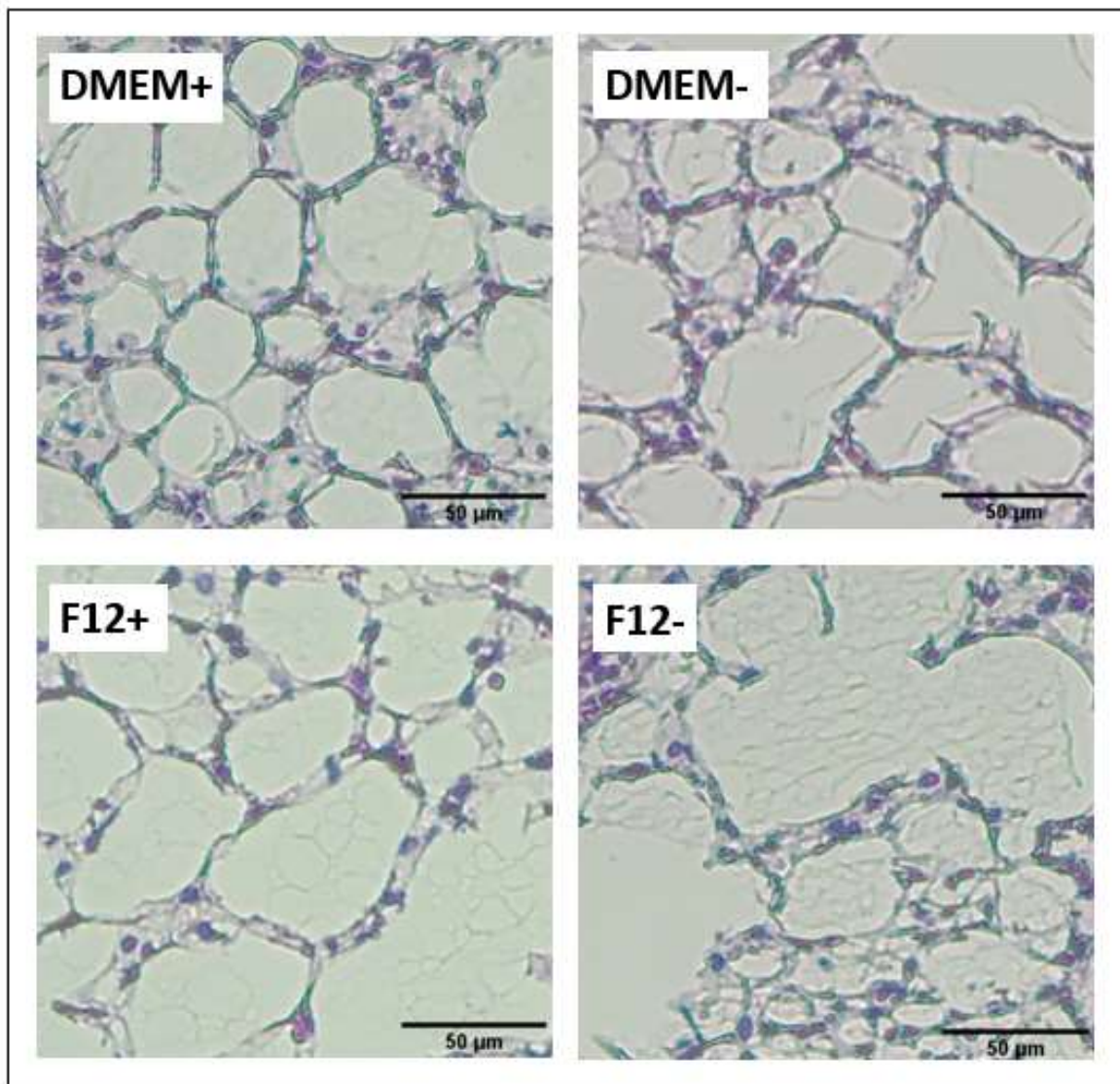
Figure 5. 4: PCLS stained with haematoxylin and eosin after 7 days of culturing. PCLS cultured in DMEM+, DMEM-, F12+ and F12- from 7 days. Objective 10×, Scale bar 50 μm, n = 2 separate mice.

5.2 Transduction of PCLS with Arl13b and ACE2 lentiviral particles

After estimating day 3 and DMEM+ were the most suitable conditions, they were used for the rest of the experiments. PCLS were transduced with Arl13b lentiviral particles to determine the possibility of using transduction for murine PCLS models. After applying three different concentrations of transduction mixtures (25%, 50% and 100%), the medium was changed after 24 hours, and the lung slices were allowed to grow for additional 48 hours before any experiment, as described in Chapter 4.6.4. The transduction efficiency was assessed by

counting the number of Arl13b-positive cells using Zeiss Spinning Disk Confocal Microscope. At least 3 slices per condition and 3 focal areas per slice were imaged.

The number of Ar13b positive cells in PCLS declined as the concentration of the transduction mixture increased. The 25% transduction mixture proved the most effective of the three concentrations. Although data in Figure 5.5B indicates that the differences between the transduction conditions were not statistically significant ($p = 0.0722$, one-way ANOVA), Figure 5.5A confirms that the highest amount of Arl13b was observed in PCLS transduced with the 25% mixture.

PCLS were also transduced with three concentrations ($0.25\times$, $0.5\times$, and $1\times$) of ACE2 lentiviral particles on day 3. Like Arl13b transduction, the transduction efficiency was quantified by counting the number of ACE2-positive cells in at least 3 slices per condition and 3 focal areas per slice.

The concentration of lentiviral particles used for transduction directly impacts the increase of ACE2-positive cells, as depicted in Figure 5.5C. The data is presented in a bar graph (Figure 5.5D), which clearly shows a gradual increase in transduced cells in PCLS, depending on the concentration used ($p = 0.0222$, one-way ANOVA). A closer look at the transduced cells is available in the upper right corner of Figure 5.5C.
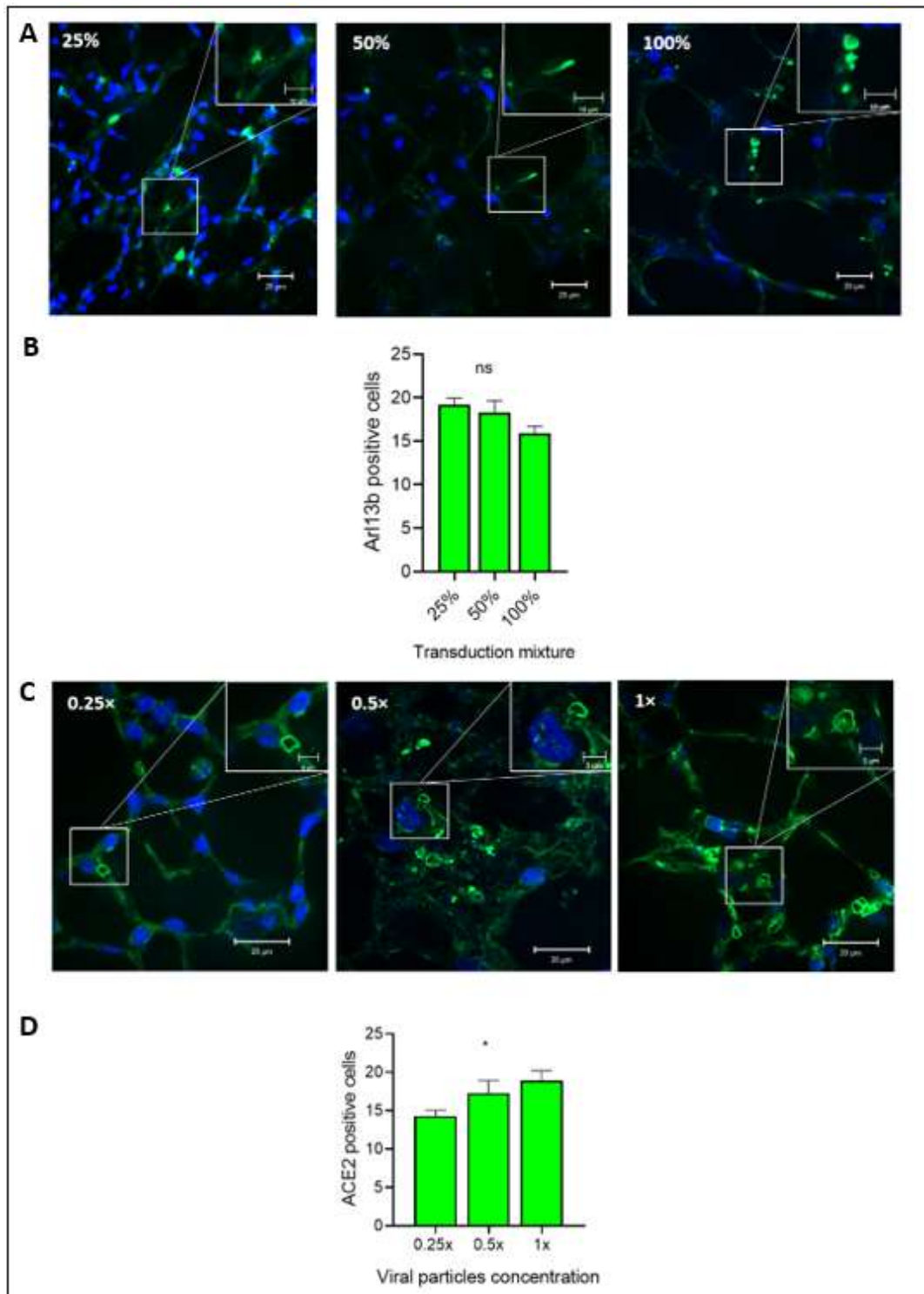
Figure 5. 5: Transduction of PCLS with Arl13b and ACE2 lentiviral particles. (A) Images of cells traduced with GFP-Arl13b in slices transduced with 25%, 50% and 100% transduction mixture. Cell nuclei are stained blue with Hoechst nuclear dye. 40× Objective, Scale bar 20 μm, scale bar in zoomed section 10 μm. (B) Quantification analysis of Arl13b transduced cell in PCLS with 25%, 50% and 100% transduction mixtures. Data are presented as mean ± SEM, n = 3 separate mice. One-way ANOVA. Not significant, ns. (C) Images of PCLS transduced with

0.25×, 0.5× and 1× ACE2 lentiviral particles. Cell nuclei are stained blue with Hoechst nuclear dye. 60× Objective, Scale bar 20 μm. The scale bar in the magnified section is 5 μm. (D) Quantification analysis of ACE2-transduced cell in PCLS. Data are presented as mean ± SEM, n = 2 separate mice. *p = 0.0222, one-way ANOVA.

5.3 Immunofluorescence staining of E-Cadherin in the lung slices after the treatment with the Cell Stimulation Cocktail.

This experiment aimed to evaluate the cytotoxicity induced by the Cell Stimulation Cocktail on PCLS. The Cell Stimulation Cocktail consists of phorbol 12-myristate 13-acetate and ionomycin, which are sufficient to induce the activation of many cell types to produce cytokines. Therefore, on day 3, the PCLS were treated to four different concentrations of the Cell Stimulation Cocktail - 0.25×, 0.5×, 1×, and 2× for 24 hours. Change in E-Cadherin expression was used as a measure to quantify the Cell Stimulation Cocktail effect. The number of E-Cadherin-positive cells per 20 000 μm^2, which appeared as green signals, was measured in at least 2-3 slices per condition and 3 focal areas per slice.

Results showed that a higher concentration of the Cell Stimulation Cocktail led to a decrease in the number of cells stained positive with E-Cadherin (Figure 5.6A). These findings were confirmed through a one-way ANOVA statistical test (****p < 0.0001), indicating statistical significance (Figure 5.6B).
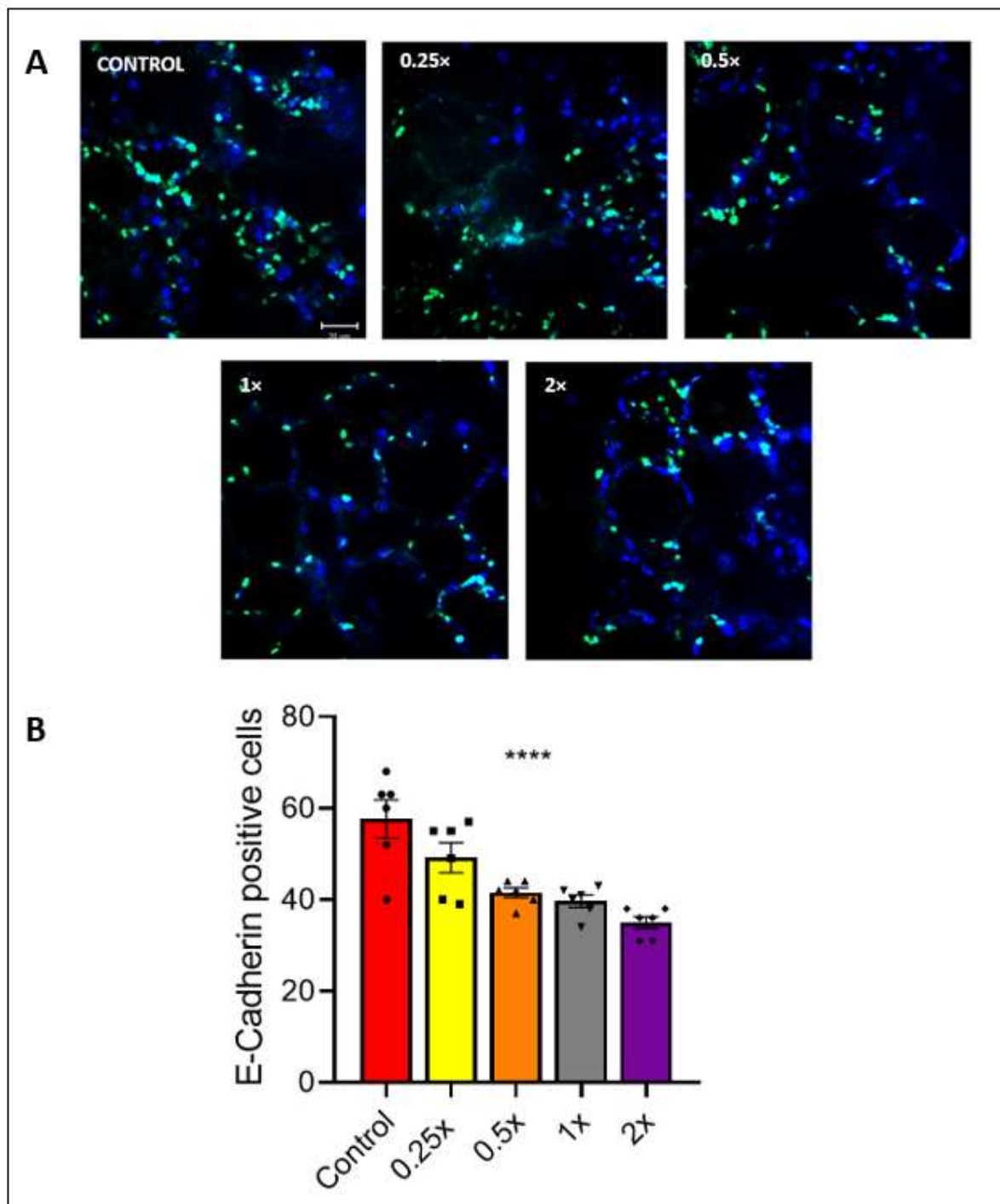
Figure 5. 6: Immunofluorescence staining of PCLS with E-Cadherin. (A) Images of PCLS showing E-Cadherin cells (green) after treatment with 0.25×, 0.5×, 1×, and 2× by the Cell Stimulation Cocktail. Cell nuclei are stained blue with Hoechst nuclear dye. 40× Objective, Scale bar 20 μm. (B) Analysis of E-Cadherin-positive cells after treatment with 0.25×, 0.5×, 1×, and 2× the Cell Stimulation Cocktail. Control is untreated. ****$p < 0.0001$, one-way ANOVA. Data are presented as mean ± SEM, n = 1 separate mouse.

5.4 Treatment of the PCLS with Methotrexate and Cyclophosphamide

5.4.1 Pre-MTS and Post-MTS analysis of PCLS

After culturing the lung slices for three days, an MTS assay was performed to assess the viability. The assay results suggest that the absorbance is higher in slices with a diameter size of 5 mm (Figure 5.7A). This is due to the higher abundance of formazan dye converted by viable cells. It is clear from the data that larger-sized PCLSs (5 mm diameter) show higher MTS absorbance compared to smaller-sized PCLSs (2.5 mm diameter). The data suggest that variability in PCLS size can affect the viability results. Thus, as much as possible, equal-sized PCLSs were utilized for the tests detailed below.

PCLS were treated with two cytotoxic agents: methotrexate (MTX) at 5, 25, and 50 µg/ml concentrations and cyclophosphamide (CP) at 10, 150, and 500 µg/ml concentrations to determine the cytotoxic effect of anticancer compounds on PCLS. A pre-MTS analysis was performed before drug treatment. Slices were then washed to remove residual MTS and treated with MTX and CP for 4 days. Following drug treatment, a post-MTS analysis was performed. The change in viability was quantified based on the pre-MTS and post-MTS absorbance readings. As shown in Figure 5.7B, the viability of the PCLS decreases with increasing concentrations of the drugs. There was no significant cytotoxicity at 5 µg/ml and 25 µg/ml MTX concentrations. However, a statistically significant change was observed at 50 µg/ml MTX. On the contrary, CP was cytotoxic at all tested concentrations, which was in line with the known pulmonary toxicity of CP (El-Kashef, 2018).
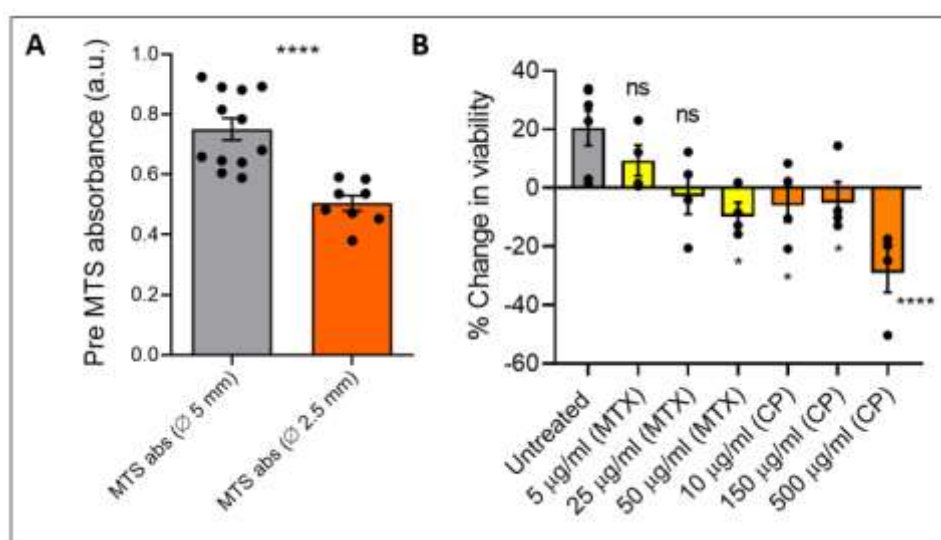
Figure 5. 7: MTS viability assay of drug-treated PCLS. (A) Pre-MTS and Post-MTS absorbances of drug-untreated PCLS of different sizes. ****p < 0.0001, unpaired t-test. Data

are presented as mean ± SEM, n = 2 separate mice. (B) The % change in viability after treatment with MTX and CP. ****$p < 0.0001$, *$p < 0.05$, One-way ANOVA. Data are presented as mean ± SEM, n = 2 separate mice.

5.4.2 Immunofluorescence staining of the lung slices after treatment with Methotrexate and Cyclophosphamide

The post-MTS treated slices were subjected to immunofluorescent labelling against E-Cadherin to detect any changes caused by the treatment. The analysis showed a significant decrease in E-Cadherin levels with increasing concentrations of MTX (Figure 5.8) and CP (Figure 5.9) compared to untreated control. To better observe the changes in E-Cadherin, each image is accompanied by a magnified view of a single cell.
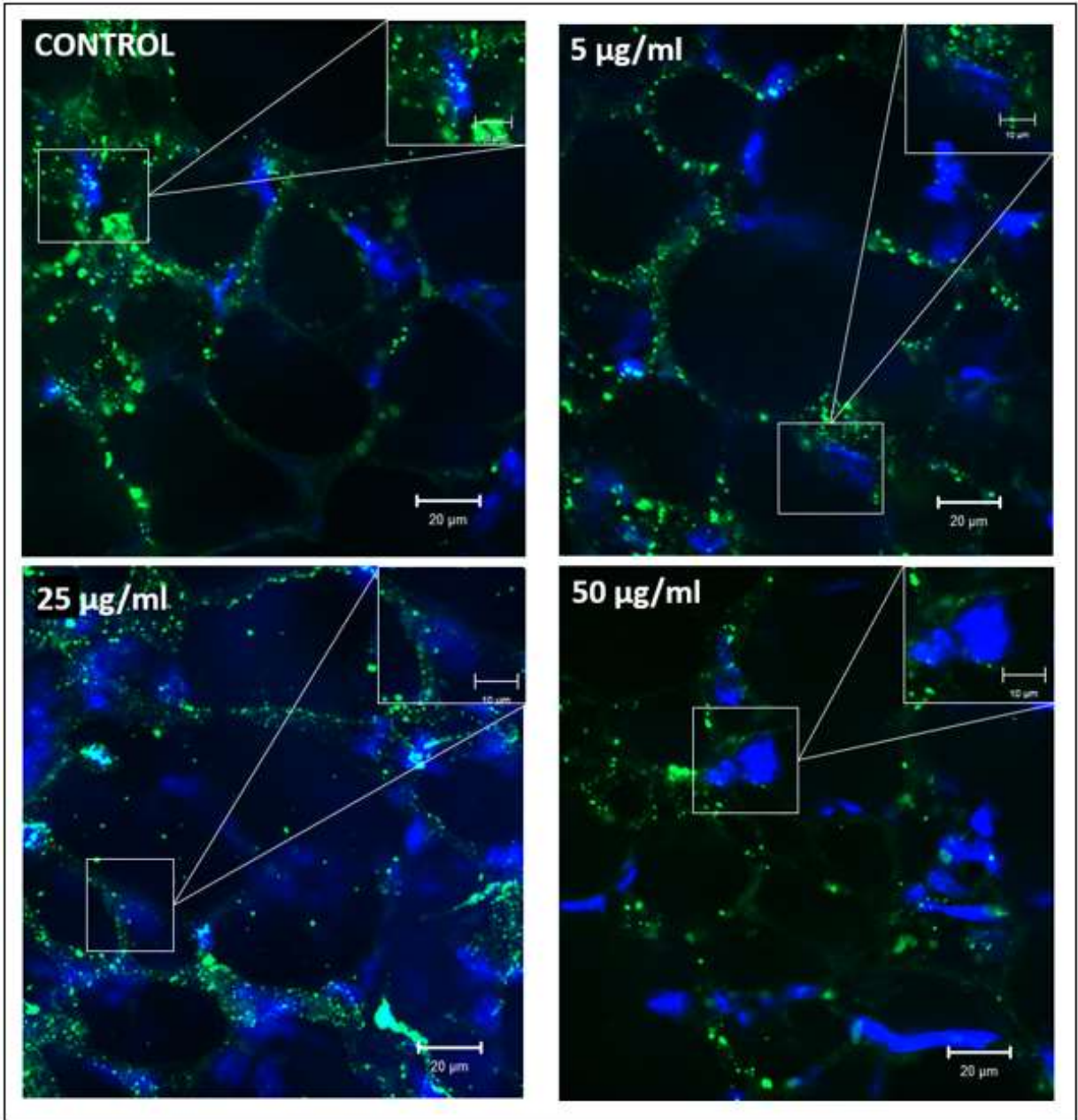
Figure 5. 8: Immunofluorescence staining of E-Cadherin of PCLS treated with 5, 25 and 50 µg/ml Methotrexate. Untreated PCLS were used as a control. Objective 40×, Scale bar 20 µm; scale bar in magnified section 10 µm.
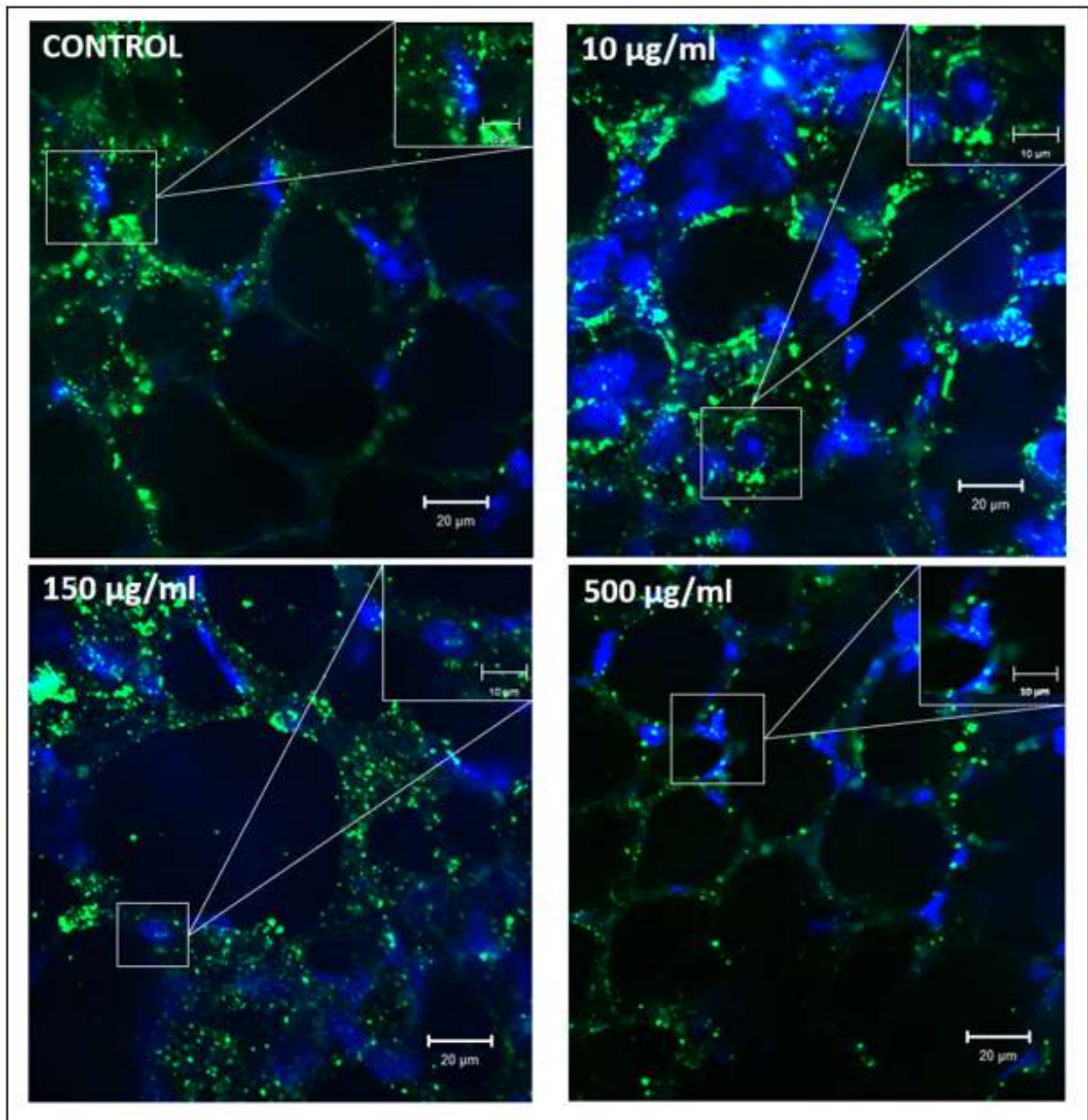
Figure 5. 9: Immunofluorescence staining of E-Cadherin of PCLS treated with 5, 25 and 50 µg/ml Methotrexate. Untreated PCLS were used as a control. Objective 40×, Scale bar 20 µm; scale bar in magnified section 10 µm.

5.4.3 Western blot analysis of E-Cadherin in MTX and CP-treated PCLS.

Following the isolation of proteins from PCLS treated with MTX and CP, an equal amount of proteins from each sample was subjected to Western blot analysis. This analysis aimed to determine any changes in E-Cadherin concentrations after treatment. Unfortunately, the Western blot analysis was unsuccessful due to improper transfer in some samples. This was evident by the absence of GAPDH bands in some samples (Figure 5.10).
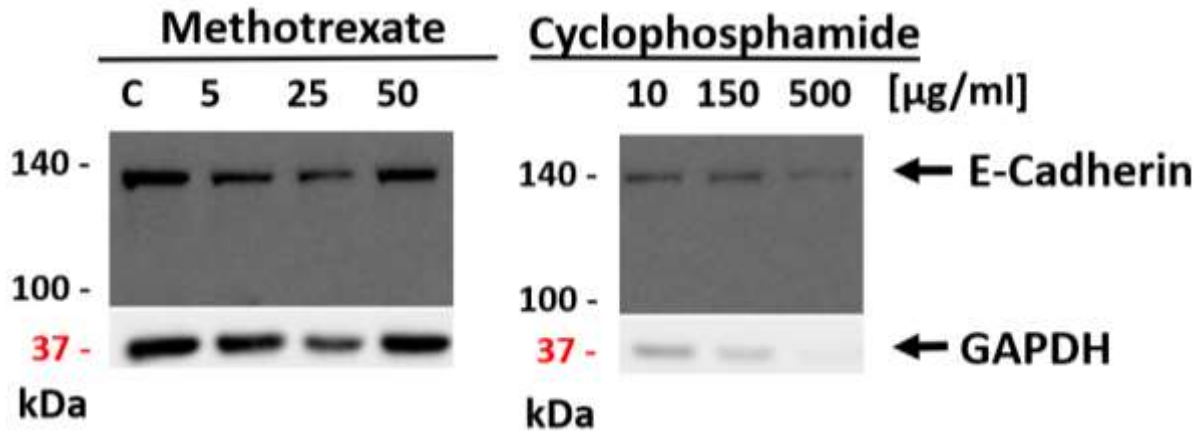
Figure 5. 10: Western blot analysis of the E-Cadherin from PCLS samples treated with Methotrexate and Cyclophosphamide. C – untreated control. GAPDH was used as a loading control. n = 2 separate mice.

6 DISCUSSION

Respiratory diseases, such as COPD, asthma, and lung cancer, are the leading cause of mortality worldwide (Viana *et al*., 2021). Unfortunately, the prevalence of these diseases is on the rise due to constant exposure to air pollutants, smoking, population ageing, and infectious organisms. As a result, the healthcare system and citizens face a significant financial burden (Wang *et al*., 2021). This burden has only been exacerbated by the recent outbreak of SARS-CoV-2, which has further highlighted the importance of respiratory research. Animal precision-cut lung slices offer a cost-effective alternative to traditional animal models and more intricate 2D and 3D models for the precise study of respiratory diseases (Viana *et al*., 2021). In this thesis, the precision-cut lung slices were developed and optimised using a vibratome for *ex vivo* experiments. A number of assays were conducted to test the potential and suitability of PCLS as a model for studying respiratory diseases.

Optimizing the culturing conditions of PCLS was crucial to ensure accurate and reliable results in subsequent experiments. The use of supplements, such as FBS, has been a topic of debate due to its potential to cause fibroblast proliferation and influence experimental outcomes, as Michalaki et al. (2022) suggested. To address this concern, many studies, including Hiorns *et al*. (2016) and Wu *et al*. (2019), have utilized serum-free medium for culturing PCLS. On the other side, Bryson *et al*. (2020) found that using a serum-free medium resulted in 30% higher cell viability in avian PCLS after 7 days of culturing. However, my observations with murine PCLS showed that adding 1% FBS increased cell viability compared to serum-free PCLS, which is consistent with the findings of Henjakovic *et al*. (2008). After conducting further histological analysis, it has been confirmed that DMEM with 1% FBS is the most appropriate medium for the experiments.

Additionally, it has been found that day 3 was the optimal time for conducting assays, as PCLS had the lowest number of dead cells. However, after day 3, the number of dead cells started to increase. This finding is supported by Li *et al*. (2020c), where the viability of PCLS was preserved for 3-7 days. It is possible that the viability and quality of the PCLS could be potentially improved by using younger mice. The mice used in this thesis ranged from 8-20 weeks old, which is difficult to culture, whereas other studies have utilized mice no older than 12 weeks old (Niehof *et al*., 2017; Puttur *et al*., 2019). The findings indicate that it is crucial to optimize the culturing conditions based on the specific assays being employed.

Previous studies have used lung slices to investigate the transduction activity of various viral vectors, as demonstrated by Griesenbach *et al*. (2012) and Gerpe *et al*. (2018). Based on

this, lentiviral transduction was deemed a suitable *ex vivo* experiment. It has been shown that VSV-G pseudotyped lentiviruses are capable of transducing mouse airway and alveolar epithelial cells, leading to consistent and long-lasting gene expression for up to 24 weeks (Rawle *et al*., 2021). In line with these findings, my results demonstrate successful lentiviral transduction of ACE2 and Arl13b. ACE2 is a receptor responsible for cell attachment and entry of SARS-CoV-2 (Rawle *et al*., 2021). Notably, the number of ACE2-positive cells was highest when using lentiviral particles with a concentration of 1×, suggesting that higher lentiviral particle concentrations lead to increased efficiency. This indicates the future possible usage of PCLS for investigating SARS-CoV-2.

ARL13B is a crucial regulatory GTPase that plays a significant role in cilia function and is highly concentrated in cilia (Gigante *et al*., 2020). Primary cilia are present in specific populations of differentiated epithelial cells, such as brain ventricles, oviducts, and airways (Jain *et al*., 2010). Interestingly, non-motile primary cilia abnormalities have been observed in patients with COPD, leading to altered epithelial differentiation (Ancel *et al*., 2021). The transduction of PCLS with Arl13b has been successfully achieved, providing a promising avenue for utilizing PCLS as a model for studying ciliopathies in airways. However, from the findings, it has been observed non-significant decrease in the efficiency of Arl13b lentiviral transduction as the percentage of transduction mixture increases. This phenomenon can be attributed to the higher portion of lentiviral particles and lower medium volume in the mixture, leading to earlier depletion of nutrients in the transduction medium. In turn, this worsens the culturing conditions and further reduces transduction efficiency.

E-Cadherin is a crucial transmembrane protein that forms a significant part of adherent junctions, facilitating cell-to-cell adhesion (Heijink *et al*., 2020). The malfunctioning of E-Cadherin, which ultimately leads to epithelial barrier dysfunction, contributes to the development of various respiratory diseases, including asthma, COPD, and idiopathic pulmonary fibrosis (Yuksel *et al*., 2021). This is why E-Cadherin has been utilized to detect epithelial cell disruption through immunofluorescence staining. In order to evaluate the potential cytotoxicity of the Cell Stimulation Cocktail and two anti-cancer drugs, Methotrexate and Cyclophosphamide, a series of experiments were conducted. The Cell Stimulation Cocktail is known to activate a variety of cell types, leading to the production of cytokines, including pro-inflammatory cytokines. Inflammation is an important mechanism for protecting cells and repairing tissues; however, it can also cause harm to healthy tissues (Rock and Kono, 2008). This was confirmed by immunofluorescence staining of E-Cadherin, as the increasing concentration of the Cell Stimulation Cocktail caused the number of E-Cadherin-positive cells

to be reduced. The effects of anti-cancer drugs Methotrexate and Cyclophosphamide, commonly used in lung cancer treatment, were observed to have a similar impact. As expected, the concentration of the drugs increased, and the viability of the cells decreased. This was confirmed through experimental data obtained from post-MTS viability assays and immunofluorescence staining of E-Cadherin. These findings suggest that the PCLS model is a reliable method for estimating cytotoxicity, as previously stated in a number of studies (Nassimi *et al*., 2009; Krabbe *et al*., 2018).

There are various methods to enhance the outcomes of experiments. One promising approach is to employ younger mice, as previously recommended. This strategy can potentially improve the viability of PCLS, thereby prolonging the culturing period. Additionally, embedding PCLS in synthetic PEG-hydrogels can extend the culturing time by providing a tailored microenvironment for cells. As demonstrated by Bailey et al. (2020), this technique can increase cultivation time by up to three weeks, which is particularly useful for more time-intensive experiments. An appropriate way to enhance future experiments would be to utilize the modular microphysiological system technology introduced by Böhlen *et al*. (2021). This technology enables longer periods of culturing with improved viability and membrane integrity, making it an ideal choice for experiments that require extended culture periods, such as repeated dose toxicity or pharmacology studies.

7 CONCLUSION

Murine precision-cut lung slices have immense potential as a model for early-stage research on respiratory diseases, especially due to human lung tissue unavailability. The primary objective of this master's thesis was to develop optimal procedures for generating murine precision-cut lung slices using the vibratome for *ex vivo* experiments. After optimization, PCLS were used to study lentiviral transduction and cytotoxicity, mainly immunofluorescence staining. Our data suggest that PCLS are a suitable model, as an alternative to human lung tissues, for *ex vivo* experiments, but culturing conditions should be considered as they may vary based on the experiment.

The versatility of PCLS offers a valuable tool to be regularly applied for cytotoxic assays with anti-cancer drugs or substances inducing inflammation. They can also be utilized for immunofluorescence protocols, lentiviral transduction, histological analysis or studying proteins extracted from lung slices using Western blot analysis. Our findings prove that PCLS are an appropriate model that can be used for multiple experimental procedures to research mechanisms of respiratory diseases or cytotoxicity and drug discovery.

8 REFERENCES

Agache, I., & Akdis, C. A. (2016). Endotypes of allergic diseases and asthma: An important step in building blocks for the future of precision medicine. *Allergology International*, *65*(3), 243–252. https://doi.org/10.1016/j.alit.2016.04.011

Agraval, H., & Chu, H. W. (2022). Lung Organoids in Smoking Research: Current Advances and Future Promises. *Biomolecules*, *12*(10), 1463. https://doi.org/10.3390/biom12101463

Akram, K. M., Yates, L. L., Mongey, R., Rothery, S., Gaboriau, D. C. A., Sanderson, J., Hind, M., Griffiths, M., & Dean, C. H. (2019). Live imaging of alveologenesis in precision-cut lung slices reveals dynamic epithelial cell behaviour. *Nature Communications*, *10*(1). https://doi.org/10.1038/s41467-019-09067-3

Alsafadi, H. N., Uhl, F. E., Pineda, R. H., Bailey, K. E., Rojas, M., Wagner, D. E., & Königshoff, M. (2020). Applications and Approaches for Three-Dimensional Precision-Cut Lung Slices. Disease Modeling and Drug Discovery. *American Journal of Respiratory Cell and Molecular Biology*, *62*(6), 681–691. https://doi.org/10.1165/rcmb.2019-0276tr

Amann, A., Zwierzina, M., Gamerith, G., Bitsche, M., Huber, J. M., Vogel, G. F., Blumer, M., Koeck, S., Pechriggl, E. J., Kelm, J. M., Hilbe, W., & Zwierzina, H. (2014). Development of an Innovative 3D Cell Culture System to Study Tumour - Stroma Interactions in Non-Small Cell Lung Cancer Cells. *PLoS ONE*, *9*(3), e92511. https://doi.org/10.1371/journal.pone.0092511

Ancel, J., Belgacemi, R., Diabasana, Z., Perotin, J., Bonnomet, A., Dewolf, M., Launois, C., Mulette, P., Deslée, G., Polette, M., & Dormoy, V. (2021). Impaired Ciliary Beat Frequency and Ciliogenesis Alteration during Airway Epithelial Cell Differentiation in COPD. *Diagnostics*, *11*(9), 1579. https://doi.org/10.3390/diagnostics11091579

Bailey, K. E., Pino, C., Lennon, M. L., Lyons, A., Jacot, J. G., Lammers, S. R., Königshoff, M., & Magin, C. M. (2020). Embedding of Precision-Cut Lung Slices in Engineered Hydrogel Biomaterials Supports Extended *Ex vivo* Culture. *American Journal of Respiratory Cell and Molecular Biology*, *62*(1), 14–22. https://doi.org/10.1165/rcmb.2019-0232ma

Barnes, P. J. (2008). Immunology of asthma and chronic obstructive pulmonary disease. *Nature Reviews Immunology*, *8*(3), 183–192. https://doi.org/10.1038/nri2254

Barnes, P. J. (2014). Cellular and Molecular Mechanisms of Chronic Obstructive Pulmonary Disease. *Clinics in Chest Medicine*, *35*(1), 71–86. https://doi.org/10.1016/j.ccm.2013.10.004

Barnes, P. J., Burney, P. G. J., Silverman, E. K., Celli, B. R., Vestbo, J., Wedzicha, J. A., & Wouters, E. F. M. (2015). Chronic obstructive pulmonary disease. *Nature Reviews Disease Primers*, *1*(1). https://doi.org/10.1038/nrdp.2015.76

Barron, S. L., Saez, J., & Owens, R. M. (2021). In Vitro Models for Studying Respiratory Host–Pathogen Interactions. *Advanced Biology*, *5*(6), 2000624. https://doi.org/10.1002/adbi.202000624

Behrsing, H. P., Furniss, M. J., Davis, M., Tomaszewski, J. E., & Parchment, R. E. (2012). In Vitro Exposure of Precision-Cut Lung Slices to 2-(4-Amino-3-Methylphenyl)-5-Fluorobenzothiazole Lysylamide Dihydrochloride (NSC 710305, Phortress) Increases Inflammatory Cytokine Content and Tissue Damage. *Toxicological Sciences*, *131*(2), 470–479. https://doi.org/10.1093/toxsci/kfs319

Bellec, J., Bacchetta, M., Losa, D., Anegon, I., Chanson, M., & Nguyen, T. (2015). <i>CFTR</i> Inactivation by Lentiviral Vector-mediated RNA Interference and CRISPR-Cas9 Genome Editing in Human Airway Epithelial Cells. *Current Gene Therapy*, *15*(5), 447–459. https://doi.org/10.2174/1566523215666150812115939

Benam, K. H., Villenave, R., Lucchesi, C., Varone, A., Hubeau, C., Lee, H. H., Alves, S. E., Salmon, M., Ferrante, T. C., Weaver, J. C., Bahinski, A., Hamilton, G. A., & Ingber, D. E. (2015). Small airway-on-a-chip enables analysis of human lung inflammation and drug responses in vitro. *Nature Methods*, *13*(2), 151–157. https://doi.org/10.1038/nmeth.3697

Białkowska, K., Komorowski, P., Bryszewska, M., & Miłowska, K. (2020). Spheroids as a Type of Three-Dimensional Cell Cultures—Examples of Methods of Preparation and the Most Important Application. *International Journal of Molecular Sciences*, *21*(17), 6225. https://doi.org/10.3390/ijms21176225

Böhlen, S., Konzok, S., Labisch, J. J., Dehmel, S., Schaudien, D., Behrens, S., Schmieder, F., Braun, A., Sonntag, F., & Sewald, K. (2021). Using a micro-physiological system to prolong the preservation of *ex vivo* lung tissue. *Current Directions in Biomedical Engineering*, *7*(2), 207–210. https://doi.org/10.1515/cdbme-2021-2053

Bonniaud, P., Fabre, A., Frossard, N., Guignabert, C., Inman, M., Kuebler, W. M., Maes, T., Shi, W., Stampfli, M., Uhlig, S., White, E., Witzenrath, M., Bellaye, P. S., Crestani, B., Eickelberg, O., Fehrenbach, H., Guenther, A., Jenkins, G., Joos, G., Kolb, M. (2018). Optimising experimental research in respiratory diseases: an ERS statement. *European Respiratory Journal*, *51*(5), 1702133. https://doi.org/10.1183/13993003.02133-2017

Brat, K., Svoboda, M., Hejduk, K., Plutinsky, M., Zatloukal, J., Volakova, E., Popelkova, P., Novotna, B., Engova, D., Franssen, F. M., Vanfleteren, L. E., Spruit, M. A., & Koblizek, V. (2021). Introducing a new prognostic instrument for long-term mortality prediction in COPD patients: the CADOT index. *Biomedical Papers*, *165*(2), 139–145. https://doi.org/10.5507/bp.2020.035

Breslin, S., & O'Driscoll, L. (2013). Three-dimensional cell culture: the missing link in drug discovery. *Drug Discovery Today*, *18*(5–6), 240–249. https://doi.org/10.1016/j.drudis.2012.10.003

Bryson, K. J., Garrido, D., Esposito, M., McLachlan, G., Digard, P., Schouler, C., Guabiraba, R., Trapp, S., & Vervelde, L. (2020). Precision cut lung slices: a novel versatile tool to examine host–pathogen interaction in the chicken lung. *Veterinary Research*, *51*(1). https://doi.org/10.1186/s13567-019-0733-0

Bush, A., & Thomson, A. H. (2007b). Acute bronchiolitis. *BMJ*, *335*(7628), 1037–1041. https://doi.org/10.1136/bmj.39374.600081.ad

Cao, X., Lin, H., Muskhelishvili, L., Latendresse, J., Richter, P., & Heflich, R. H. (2015). Tight junction disruption by cadmium in an in vitro human airway tissue model. *Respiratory Research*, *16*(1). https://doi.org/10.1186/s12931-015-0191-9

Carr, T. F., Zeki, A. A., & Kraft, M. (2018). Eosinophilic and Noneosinophilic Asthma. *American Journal of Respiratory and Critical Care Medicine*, *197*(1), 22–37. https://doi.org/10.1164/rccm.201611-2232pp

Cedilak, M., Banjanac, M., Belamarić, D., Paravić Radičević, A., Faraho, I., Ilić, K., Čužić, S., Glojnarić, I., Eraković Haber, V., & Bosnar, M. (2019). Precision-cut lung slices from bleomycin treated animals as a model for testing potential therapies for idiopathic pulmonary fibrosis. *Pulmonary Pharmacology &Amp; Therapeutics*, *55*, 75–83. https://doi.org/10.1016/j.pupt.2019.02.005

Chen, Z., Fillmore, C. M., Hammerman, P. S., Kim, C. F., & Wong, K. K. (2014). Non-small-cell lung cancers: a heterogeneous set of diseases. *Nature Reviews Cancer*, *14*(8), 535–546. https://doi.org/10.1038/nrc3775

Chronic Obstructive Lung Disease, Global Initiative for. (2017). *Pocket Guide to COPD Diagnosis, Management and Prevention: A Guide for Healthcar (2018)*. CreateSpace Independent Publishing Platform.

Cidem, A., Bradbury, P., Traini, D., & Ong, H. X. (2020). Modifying and Integrating in vitro and *ex vivo* Respiratory Models for Inhalation Drug Screening. *Frontiers in Bioengineering and Biotechnology*, *8*. https://doi.org/10.3389/fbioe.2020.581995

Cilloniz, C., Ewig, S., Polverino, E., Marcos, M. A., Esquinas, C., Gabarrus, A., Mensa, J., & Torres, A. (2011). Microbial aetiology of community-acquired pneumonia and its relation to severity. *Thorax*, *66*(4), 340–346. https://doi.org/10.1136/thx.2010.143982

Clark, T. W., Medina, M. J., Batham, S., Curran, M. D., Parmar, S., & Nicholson, K. G. (2014). Adults hospitalised with acute respiratory illness rarely have detectable bacteria in the absence of COPD or pneumonia; viral infection predominates in a large prospective UK sample. *Journal of Infection*, *69*(5), 507–515. https://doi.org/10.1016/j.jinf.2014.07.023

Cohen, M., Levine, S. M., & Zar, H. J. (2022). World Lung Day: impact of "the big 5 lung diseases" in the context of COVID-19. *American Journal of Physiology-Lung Cellular and Molecular Physiology*, *323*(3), L338–L340. https://doi.org/10.1152/ajplung.00261.2022

Correia, W., Dorta-Guerra, R., Sanches, M., Almeida Semedo, C. D. J. B., Valladares, B., de Pina-Araújo, I. I. M., & Carmelo, E. (2021). Study of the Etiology of Acute Respiratory Infections in Children Under 5 Years at the Dr. Agostinho Neto Hospital, Praia, Santiago Island, Cabo Verde. *Frontiers in Pediatrics*, *9*. https://doi.org/10.3389/fped.2021.716351

Crowley, G., Kwon, S., Caraher, E. J., Haider, S., Lam, R., Batra, P., Melles, D., Liu, M., & Nolan, A. (2019). Quantitative lung morphology: semi-automated measurement of mean linear intercept. *BMC Pulmonary Medicine*, *19*(1). https://doi.org/10.1186/s12890-019-0915-6

Dalziel, S. R., Haskell, L., O'Brien, S., Borland, M. L., Plint, A. C., Babl, F. E., & Oakley, E. (2022). Bronchiolitis. *The Lancet*, *400*(10349), 392–406. https://doi.org/10.1016/s0140-6736(22)01016-9

Danov, O., Jiménez Delgado, S. M., Obernolte, H., Seehase, S., Dehmel, S., Braubach, P., Fieguth, H. G., Matschiner, G., Fitzgerald, M., Jonigk, D., Knauf, S., Pfennig, O., Warnecke, G., Wichmann, J., Braun, A., & Sewald, K. (2018). Human lung tissue provides highly relevant data about efficacy of new anti-asthmatic drugs. *PLOS ONE*, *13*(11), e0207767. https://doi.org/10.1371/journal.pone.0207767

Das, V., Bruzzese, F., Konečný, P., Iannelli, F., Budillon, A., & Hajdúch, M. (2015). Pathophysiologically relevant in vitro tumour models for drug screening. *Drug Discovery Today*, *20*(7), 848–855. https://doi.org/10.1016/j.drudis.2015.04.004

Dong, M., Philippi, C., Loretz, B., Nafee, N., Schaefer, U. F., Friedel, G., Ammon-Treiber, S., Griese, E. U., Lehr, C. M., Klotz, U., & Mürdter, T. E. (2011). Tissue slice model of human lung cancer to investigate telomerase inhibition by nanoparticle delivery of antisense 2′-O-methyl-RNA. *International Journal of Pharmaceutics*, *419*(1–2), 33–42. https://doi.org/10.1016/j.ijpharm.2011.07.009

Donnelly, L. E., & Barnes, P. J. (2006). Chemokine receptors as therapeutic targets in chronic obstructive pulmonary disease. *Trends in Pharmacological Sciences*, *27*(10), 546–553. https://doi.org/10.1016/j.tips.2006.08.001

Dvorak, A., Tilley, A. E., Shaykhiev, R., Wang, R., & Crystal, R. G. (2011). Do Airway Epithelium Air–Liquid Cultures Represent the *In vivo* Airway Epithelium Transcriptome? *American Journal of Respiratory Cell and Molecular Biology*, *44*(4), 465–473. https://doi.org/10.1165/rcmb.2009-0453oc

Efstathiou, C., Abidi, S. H., Harker, J., & Stevenson, N. J. (2020). Revisiting respiratory syncytial virus's interaction with host immunity, towards novel therapeutics. *Cellular and Molecular Life Sciences*, *77*(24), 5045–5058. https://doi.org/10.1007/s00018-020-03557-0

Elbarbary, M., Oganesyan, A., Honda, T., Kelly, P., Zhang, Y., Guo, Y., Morgan, G., Guo, Y., & Negin, J. (2020). Ambient air pollution, lung function and COPD: cross-sectional analysis from the WHO Study of AGEing and adult health wave 1. *BMJ Open Respiratory Research*, *7*(1), e000684. https://doi.org/10.1136/bmjresp-2020-000684

European Lung Foundation. (2021, July 27). *Acute Lower Respiratory Tract Infection|Diagnosis & Treatment|ELF*. Retrieved December 3, 2022, from https://europeanlung.org/en/information-hub/lung-conditions/acute-lower-respiratory-infections/

Fan, R., Wen, B., Liu, W., Zhang, J., Liu, C., Fan, C., & Qu, X. (2018b). Altered regulatory cytokine profiles in cases of pediatric respiratory syncytial virus infection. *Cytokine*, *103*, 57–62. https://doi.org/10.1016/j.cyto.2017.12.028

Fang, Y., & Eglen, R. M. (2017). Three-Dimensional Cell Cultures in Drug Discovery and Development. *SLAS Discovery*, *22*(5), 456–472. https://doi.org/10.1177/1087057117696795

Felgenhauer, U., Schoen, A., Gad, H. H., Hartmann, R., Schaubmar, A. R., Failing, K., Drosten, C., & Weber, F. (2020). Inhibition of SARS–CoV-2 by type I and type III interferons. *Journal of Biological Chemistry*, *295*(41), 13958–13964. https://doi.org/10.1074/jbc.ac120.013788

Forum of International Respiratory Societies. (2021). The global impact of respiratory disease. Third Edition. European Respiratory Society. Accessed 22 September, 2021. firsnet.org/images/publications/FIRS_Master_09202021.pdf

Francis, I., Shrestha, J., Paudel, K. R., Hansbro, P. M., Warkiani, M. E., & Saha, S. C. (2022). Recent advances in lung-on-a-chip models. *Drug Discovery Today*, *27*(9), 2593–2602. https://doi.org/10.1016/j.drudis.2022.06.004

Gan, W. Q. (2004). Association between chronic obstructive pulmonary disease and systemic inflammation: a systematic review and a meta-analysis. *Thorax*, *59*(7), 574–580. https://doi.org/10.1136/thx.2003.019588

Geiger, N., König, E., Oberwinkler, H., Roll, V., Diesendorf, V., Fähr, S., Obernolte, H., Seewald, K., Wronski, S., Steinke, M., & Bodem, J. (2022). Acetylsalicylic acid and Salicylic acid inhibit SARS-CoV-2 replication in precision-cut lung slices. *BioRxiv (Cold Spring Harbor Laboratory)*. https://doi.org/10.1101/2022.08.09.503270

Gerhards, N. M., Cornelissen, J. B. W. J., Van Keulen, L. J. M., Harders-Westerveen, J., Vloet, R., Smid, B., Vastenhouw, S., Van Oort, S., Hakze-van Der Honing, R. W., Gonzales, J. L., Stockhofe-Zurwieden, N., De Jong, R., Van Der Poel, W. H. M., Vreman, S., Kortekaas, J., Wichgers Schreur, P. J., & Oreshkova, N. (2021). Predictive Value of Precision-Cut Lung Slices for the Susceptibility of Three Animal Species for SARS-CoV-2 and Validation in a Refined Hamster Model. *Pathogens*, *10*(7), 824. https://doi.org/10.3390/pathogens10070824

Gerpe, M. C. R., Van Vloten, J. P., Santry, L. A., De Jong, J., Mould, R. C., Pelin, A., Bell, J., Bridle, B. W., & Wootton, S. K. (2018). Use of Precision-Cut Lung Slices as an *Ex vivo* Tool for Evaluating Viruses and Viral Vectors for Gene and Oncolytic Therapy. *Molecular Therapy. Methods & Clinical Development*, *10*, 245–256. https://doi.org/10.1016/j.omtm.2018.07.010

Gigante, E. D., Taylor, M., Ivanova, A. O., Kahn, R. A., & Caspary, T. (2020). ARL13B regulates Sonic hedgehog signaling from outside primary cilia. *ELife*, *9*. https://doi.org/10.7554/elife.50434

Gkatzis, K., Taghizadeh, S., Huh, D., Stainier, D. Y., & Bellusci, S. (2018). Use of three-dimensional organoids and lung-on-a-chip methods to study lung development, regeneration

and disease. *European Respiratory Journal*, *52*(5), 1800876. https://doi.org/10.1183/13993003.00876-2018

Gordon, E. D., Simpson, L. J., Rios, C. L., Ringel, L., Lachowicz-Scroggins, M. E., Peters, M. C., Wesolowska-Andersen, A., Gonzalez, J. R., MacLeod, H. J., Christian, L. S., Yuan, S., Barry, L., Woodruff, P. G., Ansel, K. M., Nocka, K., Seibold, M. A., & Fahy, J. V. (2016). Alternative splicing of interleukin-33 and type 2 inflammation in asthma. *Proceedings of the National Academy of Sciences*, *113*(31), 8765–8770. https://doi.org/10.1073/pnas.1601914113

Gras, D., Martinez-Anton, A., Bourdin, A., Garulli, C., de Senneville, L., Vachier, I., Vitte, J., & Chanez, P. (2017). Human bronchial epithelium orchestrates dendritic cell activation in severe asthma. *European Respiratory Journal*, *49*(3), 1602399. https://doi.org/10.1183/13993003.02399-2016

Griesenbach, U., Inoue, M., Meng, C., Farley, R., Chan, M., Newman, N. K., Brum, A., You, J., Kerton, A., Shoemark, A., Boyd, A. W., Davies, J. C., Higgins, T. E., Gill, D. R., Hyde, S. T., Innes, J. F., Porteous, D. J., Hasegawa, M., & Alton, E. W. (2012). Assessment of F/HN-Pseudotyped Lentivirus as a Clinically Relevant Vector for Lung Gene Therapy. *American Journal of Respiratory and Critical Care Medicine*, *186*(9), 846–856. https://doi.org/10.1164/rccm.201206-1056oc

Griffin, K. H., Fok, S. W., & Kent Leach, J. (2022). Strategies to capitalize on cell spheroid therapeutic potential for tissue repair and disease modeling. *Npj Regenerative Medicine*, *7*(1). https://doi.org/10.1038/s41536-022-00266-z

Habanjar, O., Diab-Assaf, M., Caldefie-Chezet, F., & Delort, L. (2021). 3D Cell Culture Systems: Tumor Application, Advantages, and Disadvantages. *International Journal of Molecular Sciences*, *22*(22), 12200. https://doi.org/10.3390/ijms222212200

Hammad, H., & Lambrecht, B. N. (2021). The basic immunology of asthma. *Cell*, *184*(6), 1469–1485. https://doi.org/10.1016/j.cell.2021.02.016

Han, Y., Duan, X., Yang, L., Nilsson-Payant, B. E., Wang, P., Duan, F., Tang, X., Yaron, T. M., Zhang, T., Uhl, S., Bram, Y., Richardson, C., Zhu, J., Zhao, Z., Redmond, D., Houghton, S., Nguyen, D. H. T., Xu, D., Wang, X., . . . Chen, S. (2020). Identification of SARS-CoV-2 inhibitors using lung and colonic organoids. *Nature*, *589*(7841), 270–275. https://doi.org/10.1038/s41586-020-2901-9

Heijink, I. H., Kuchibhotla, V. N. S., Roffel, M. P., Maes, T., Knight, D. A., Sayers, I., & Nawijn, M. C. (2020). Epithelial cell dysfunction, a major driver of asthma development. *Allergy*, *75*(8), 1902–1917. https://doi.org/10.1111/all.14421

Henjakovic, M., Sewald, K., Switalla, S., Kaiser, D., Müller, M. J., Veres, T. Z., Martin, C., Uhlig, S., Krug, N., & Braun, A. (2008). *Ex vivo* testing of immune responses in precision-cut lung slices. *Toxicology and Applied Pharmacology*, *231*(1), 68–76. https://doi.org/10.1016/j.taap.2008.04.003

Henz Ryen, A., Göls, T., Steinmetz, J., Tahir, A., Jakobsson, P. J., Backlund, A., Urban, E., & Glasl, S. (2020b). Bisabolane sesquiterpenes from the leaves of Lindera benzoin reduce prostaglandin E2 formation in A549 cells. *Phytochemistry Letters*, *38*, 6–11. https://doi.org/10.1016/j.phytol.2020.04.015

Hiemstra, P. S., Grootaers, G., van der Does, A. M., Krul, C. A., & Kooter, I. M. (2018). Human lung epithelial cell cultures for analysis of inhaled toxicants: Lessons learned and future directions. *Toxicology in Vitro*, *47*, 137–146. https://doi.org/10.1016/j.tiv.2017.11.005

Hiemstra, P. S., Tetley, T. D., & Janes, S. M. (2019). Airway and alveolar epithelial cells in culture. *European Respiratory Journal*, *54*(5), 1900742. https://doi.org/10.1183/13993003.00742-2019

Hiorns, J. E., Bidan, C. M., Jensen, O. E., Gosens, R., Kistemaker, L. E. M., Fredberg, J. J., Butler, J., Krishnan, R., & Brook, B. S. (2016). Airway and Parenchymal Strains during Bronchoconstriction in the Precision Cut Lung Slice. *Frontiers in Physiology*, *7*. https://doi.org/10.3389/fphys.2016.00309

Hofer, M., & Lutolf, M. P. (2021). Engineering organoids. *Nature Reviews Materials*, *6*(5), 402–420. https://doi.org/10.1038/s41578-021-00279-y

Huh, D., Leslie, D. C., Matthews, B. D., Fraser, J. P., Jurek, S., Hamilton, G. A., Thorneloe, K. S., McAlexander, M. A., & Ingber, D. E. (2012). A Human Disease Model of Drug Toxicity–Induced Pulmonary Edema in a Lung-on-a-Chip Microdevice. *Science Translational Medicine*, *4*(159). https://doi.org/10.1126/scitranslmed.3004249

Huh, D., Matthews, B. D., Mammoto, A., Montoya-Zavala, M., Hsin, H. Y., & Ingber, D. E. (2010). Reconstituting Organ-Level Lung Functions on a Chip. *Science*, *328*(5986), 1662–1668. https://doi.org/10.1126/science.1188302

Hynes, J., Marshall, L., Adcock, I., Novotny, T., Nic, M., Dibusz, K. and Gribaldo, L. (2020) *Advanced Non-animal Models in Biomedical Research: Respiratory Tract Diseases*, EUR 30334 EN, Publications Office of the European Union, Luxembourg, ISBN 978-92-76-21380-2, doi:10.2760/725821, JRC118161

Iakobachvili, N., Leon-Icaza, S. A., Knoops, K., Sachs, N., Mazères, S., Simeone, R., Peixoto, A., Bernard, C., Murris-Espin, M., Mazières, J., Cam, K., Chalut, C., Guilhot, C., López-Iglesias, C., Ravelli, R. B. G., Neyrolles, O., Meunier, E., Lugo-Villarino, G., Clevers, H., . . . Peters, P. (2021). Mycobacteria–host interactions in human bronchiolar airway organoids. *Molecular Microbiology*, *117*(3), 682–692. https://doi.org/10.1111/mmi.14824

Jain, R., Pan, J., Driscoll, J. F., Wisner, J. W., Huang, T., Gunsten, S. P., You, Y., & Brody, S. L. (2010). Temporal Relationship between Primary and Motile Ciliogenesis in Airway Epithelial Cells. *American Journal of Respiratory Cell and Molecular Biology*, *43*(6), 731–739. https://doi.org/10.1165/rcmb.2009-0328oc

Jensen, C., & Teng, Y. (2020). Is It Time to Start Transitioning From 2D to 3D Cell Culture? *Frontiers in Molecular Biosciences*, *7*. https://doi.org/10.3389/fmolb.2020.00033

Jordao, L., & Vieira, O. V. (2011). Tuberculosis: New Aspects of an Old Disease. *International Journal of Cell Biology*, *2011*, 1–13. https://doi.org/10.1155/2011/403623

Kapałczyńska, M., Kolenda, T., Przybyła, W., Zajączkowska, M., Teresiak, A., Filas, V., Ibbs, M., Bliźniak, R., Łuczewski, U., & Lamperska, K. (2016). 2D and 3D cell cultures – a comparison of different types of cancer cell cultures. *Archives of Medical Science*. https://doi.org/10.5114/aoms.2016.63743

Khan, M. M., Poeckel, D., Halavatyi, A., Zukowska-Kasprzyk, J., Stein, F., Vappiani, J., Sevin, D. C., Tischer, C., Zinn, N., Eley, J. D., Gudmann, N. S., Muley, T., Winter, H., Fisher, A. J., Nanthakumar, C. B., Bergamini, G., & Pepperkok, R. (2020). An integrated multiomic and quantitative label-free microscopy-based approach to study pro-fibrotic signalling in *ex vivo* human precision-cut lung slices. *European Respiratory Journal*, *58*(1), 2000221. https://doi.org/10.1183/13993003.00221-2020

Kim, J., Koo, B. K., & Knoblich, J. A. (2020). Human organoids: model systems for human biology and medicine. *Nature Reviews Molecular Cell Biology*, *21*(10), 571–584. https://doi.org/10.1038/s41580-020-0259-3

Kim, M., Mun, H., Sung, C. O., Cho, E. J., Jeon, H. J., Chun, S. M., Jung, D. J., Shin, T. H., Jeong, G. S., Kim, D. K., Choi, E. K., Jeong, S. Y., Taylor, A. M., Jain, S., Meyerson, M., & Jang, S. J. (2019). Patient-derived lung cancer organoids as in vitro cancer models for therapeutic screening. *Nature Communications*, *10*(1). https://doi.org/10.1038/s41467-019-11867-6

Kinkade, S., & Long, N. A. (2016). Acute Bronchitis. *American family physician*, *94*(7), 560–565.

Krabbe, J., Esser, A., Kanzler, S., Braunschweig, T., Kintsler, S., Spillner, J., Schröder, T., Kalverkamp, S., Balakirski, G., Gerhards, B., Rieg, A. D., Kraus, T., Brand, P., & Martin, C. (2018). The effects of zinc- and copper-containing welding fumes on murine, rat and human precision-cut lung slices. *Journal of Trace Elements in Medicine and Biology*, *49*, 192–201. https://doi.org/10.1016/j.jtemb.2018.03.008

Kuhdari, P., Brosio, F., Malaventura, C., Stefanati, A., Orsi, A., Icardi, G., & Gabutti, G. (2018). Human respiratory syncytial virus and hospitalization in young children in Italy. *Italian Journal of Pediatrics*, *44*(1). https://doi.org/10.1186/s13052-018-0492-y

Kutter, J. S., Spronken, M. I., Fraaij, P. L., Fouchier, R. A., & Herfst, S. (2018). Transmission routes of respiratory viruses among humans. *Current Opinion in Virology*, *28*, 142–151. https://doi.org/10.1016/j.coviro.2018.01.001

Lambrecht, B. N., & Hammad, H. (2014). The immunology of asthma. *Nature Immunology*, *16*(1), 45–56. https://doi.org/10.1038/ni.3049

Langhans, S. A. (2018). Three-Dimensional in Vitro Cell Culture Models in Drug Discovery and Drug Repositioning. *Frontiers in Pharmacology*, *9*. https://doi.org/10.3389/fphar.2018.00006

Larsen, J. E., & Minna, J. D. (2011). Molecular Biology of Lung Cancer: Clinical Implications. *Clinics in Chest Medicine*, *32*(4), 703–740. https://doi.org/10.1016/j.ccm.2011.08.003

Lehr, C. M., Yeo, L., & Sznitman, J. (2021). Editorial: Innovative In Vitro Models for Pulmonary Physiology and Drug Delivery in Health and Disease. *Frontiers in Bioengineering and Biotechnology*, *9*. https://doi.org/10.3389/fbioe.2021.788682

Li, G., Cohen, J. A., Martines, C., Ram-Mohan, S., Brain, J. D., Krishnan, R., Ai, X., & Bai, Y. (2020). Preserving Airway Smooth Muscle Contraction in Precision-Cut Lung Slices. *Scientific Reports*, *10*(1). https://doi.org/10.1038/s41598-020-63225-y

Li, G., Cohen, J. D., Martines, C., Ram-Mohan, S., Brain, J. D., Krishnan, R., Ai, X., & Bai, Y. (2020c). Preserving Airway Smooth Muscle Contraction in Precision-Cut Lung Slices. *Scientific Reports*, *10*(1). https://doi.org/10.1038/s41598-020-63225-y

Lin, P. L., Ford, C. B., Coleman, M. T., Myers, A. J., Gawande, R., Ioerger, T., Sacchettini, J., Fortune, S. M., & Flynn, J. L. (2013). Sterilization of granulomas is common in active and latent tuberculosis despite within-host variability in bacterial killing. *Nature Medicine*, *20*(1), 75–79. https://doi.org/10.1038/nm.3412

Lindberg, A., Lindberg, L., Sawalha, S., Nilsson, U., Stridsman, C., Lundbäck, B., & Backman, H. (2021). Large underreporting of COPD as cause of death-results from a

population-based cohort study. *Respiratory Medicine*, *186*, 106518. https://doi.org/10.1016/j.rmed.2021.106518

Liu, G., Betts, C., Cunoosamy, D. M., Åberg, P. M., Hornberg, J. J., Sivars, K. B., & Cohen, T. S. (2019). Use of precision-cut lung slices as a translational model for the study of lung biology. *Respiratory Research*, *20*(1). https://doi.org/10.1186/s12931-019-1131-x

Ma, C., Peng, Y., Li, H., & Chen, W. (2021). Organ-on-a-Chip: A New Paradigm for Drug Development. *Trends in Pharmacological Sciences*, *42*(2), 119–133. https://doi.org/10.1016/j.tips.2020.11.009

Malhotra, J., Malvezzi, M., Negri, E., La Vecchia, C., & Boffetta, P. (2016). Risk factors for lung cancer worldwide. *European Respiratory Journal*, *48*(3), 889–902. https://doi.org/10.1183/13993003.00359-2016

Michalaki, C., Dean, C. H., & Johansson, C. (2022). The Use of Precision-Cut Lung Slices for Studying Innate Immunity to Viral Infections. *Current Protocols*, *2*(8). https://doi.org/10.1002/cpz1.505

Miller, A. J., & Spence, J. R. (2017). In Vitro Models to Study Human Lung Development, Disease and Homeostasis. *Physiology*, *32*(3), 246–260. https://doi.org/10.1152/physiol.00041.2016

Moreira, A., Müller, M., Costa, P. F., & Kohl, Y. (2021). Advanced In Vitro Lung Models for Drug and Toxicity Screening: The Promising Role of Induced Pluripotent Stem Cells. *Advanced Biology*, *6*(2), 2101139. https://doi.org/10.1002/adbi.202101139

Na, F., Pan, X., Chen, J., Chen, X., Wang, M., Chi, P., You, L., Zhang, L., Zhong, A., Zhao, L., Dai, S., Zhang, M., Wang, Y., Wang, B., Zheng, J., Wang, Y., Xu, J., Wang, J., Wu, B., . . . Chen, C. (2022b). KMT2C deficiency promotes small cell lung cancer metastasis through DNMT3A-mediated epigenetic reprogramming. *Nature Cancer*, *3*(6), 753–767. https://doi.org/10.1038/s43018-022-00361-6

Närhi, K., Nagaraj, A. S., Parri, E., Turkki, R., van Duijn, P. W., Hemmes, A., Lahtela, J., Uotinen, V., Mäyränpää, M. I., Salmenkivi, K., Räsänen, J., Linder, N., Trapman, J., Rannikko, A., Kallioniemi, O., Af Hällström, T. M., Lundin, J., Sommergruber, W., Anders, S., & Verschuren, E. W. (2018). Spatial aspects of oncogenic signalling determine the response to combination therapy in slice explants from *Kras* -driven lung tumours. *The Journal of Pathology*, *245*(1), 101–113. https://doi.org/10.1002/path.5059

Nassimi, M., Schleh, C., Lauenstein, H., Hussein, R., Lübbers, K., Pohlmann, G., Switalla, S., Sewald, K., Müller, M., Krug, N., Müller-Goymann, C. C., & Braun, A. (2009). Low cytotoxicity of solid lipid nanoparticles in*in vitro*and*ex vivo*lung models. *Inhalation Toxicology*, *21*(sup1), 104–109. https://doi.org/10.1080/08958370903005769

National Cancer Institute. (n.d.). *NCI Dictionary of Cancer Terms*. Retrieved November 12, 2022, from https://www.cancer.gov/publications/dictionaries/cancer-terms/def/respiratory-disease

National Institute of Environmental Health Sciences. (n.d.). *Lung Diseases*. Retrieved November 12, 2022, from https://www.niehs.nih.gov/health/topics/conditions/lung-disease/index.cfm

Niehof, M., Hildebrandt, T., Danov, O., Arndt, K., Koschmann, J., Dahlmann, F., Hansen, T., & Sewald, K. (2017). RNA isolation from precision-cut lung slices (PCLS) from different species. *BMC Research Notes*, *10*(1). https://doi.org/10.1186/s13104-017-2447-6

Niemeyer, B. F., Zhao, P., Tuder, R. M., & Benam, K. H. (2018). Advanced Microengineered Lung Models for Translational Drug Discovery. *SLAS Discovery*, *23*(8), 777–789. https://doi.org/10.1177/2472555218760217

Nikolic, M., Sustersic, T., & Filipovic, N. (2018). In vitro Models and On-Chip Systems: Biomaterial Interaction Studies With Tissues Generated Using Lung Epithelial and Liver Metabolic Cell Lines. *Frontiers in Bioengineering and Biotechnology*, *6*. https://doi.org/10.3389/fbioe.2018.00120

Pai, M., Behr, M. A., Dowdy, D., Dheda, K., Divangahi, M., Boehme, C. C., Ginsberg, A., Swaminathan, S., Spigelman, M., Getahun, H., Menzies, D., & Raviglione, M. (2016). Tuberculosis. *Nature Reviews Disease Primers*, *2*(1). https://doi.org/10.1038/nrdp.2016.76

Peters, M. C., & Wenzel, S. E. (2020). Intersection of biology and therapeutics: type 2 targeted therapeutics for adult asthma. *The Lancet*, *395*(10221), 371–383. https://doi.org/10.1016/s0140-6736(19)33005-3

Peters, M. C., Ringel, L., Dyjack, N., Herrin, R., Woodruff, P. G., Rios, C., O'Connor, B., Fahy, J. V., & Seibold, M. A. (2019). A Transcriptomic Method to Determine Airway Immune Dysfunction in T2-High and T2-Low Asthma. *American Journal of Respiratory and Critical Care Medicine*, *199*(4), 465–477. https://doi.org/10.1164/rccm.201807-1291oc

Pezzulo, A. A., Starner, T. D., Scheetz, T. E., Traver, G. L., Tilley, A. E., Harvey, B. G., Crystal, R. G., McCray, P. B., & Zabner, J. (2011). The air-liquid interface and use of primary cell cultures are important to recapitulate the transcriptional profile of *in vivo* airway epithelia. *American Journal of Physiology-Lung Cellular and Molecular Physiology*, *300*(1), L25–L31. https://doi.org/10.1152/ajplung.00256.2010

Preuß, E. B., Schubert, S., Werlein, C., Stark, H., Braubach, P., Höfer, A., Plucinski, E. K., Shah, H. R., Geffers, R., Sewald, K., Braun, A., Jonigk, D. D., & Kühnel, M. P. (2022). The Challenge of Long-Term Cultivation of Human Precision-Cut Lung Slices. *The American Journal of Pathology*, *192*(2), 239–253. https://doi.org/10.1016/j.ajpath.2021.10.020

Puttur, F., Denney, L., Gregory, L. G., Vuononvirta, J., Oliver, R., Entwistle, L. J., Walker, S. A., Headley, M. B., McGhee, E. J., Pease, J. E., Krummel, M. F., Carlin, L. M., & Lloyd, C. M. (2019). Pulmonary environmental cues drive group 2 innate lymphoid cell dynamics in mice and humans. *Science Immunology*, *4*(36). https://doi.org/10.1126/sciimmunol.aav7638

Quinton, L. J., Walkey, A. J., & Mizgerd, J. P. (2018). Integrative Physiology of Pneumonia. *Physiological Reviews*, *98*(3), 1417–1464. https://doi.org/10.1152/physrev.00032.2017

Rabe, K. F., Hurd, S., Anzueto, A., Barnes, P. J., Buist, S. A., Calverley, P., Fukuchi, Y., Jenkins, C., Rodriguez-Roisin, R., van Weel, C., & Zielinski, J. (2007). Global Strategy for the Diagnosis, Management, and Prevention of Chronic Obstructive Pulmonary Disease. *American Journal of Respiratory and Critical Care Medicine*, *176*(6), 532–555. https://doi.org/10.1164/rccm.200703-456so

Rawle, D. J., Le, T., Dumenil, T., Yan, K., Tang, B., Nguyen, W., Watterson, D., Modhiran, N., Hobson-Peters, J., Bishop, C., & Suhrbier, A. (2021). ACE2-lentiviral transduction enables mouse SARS-CoV-2 infection and mapping of receptor interactions. *PLOS Pathogens*, *17*(7), e1009723. https://doi.org/10.1371/journal.ppat.1009723

Rehman, A. U., Hassali, M. a. A., Muhammad, S. A., Harun, S. N., Shah, S., & Abbas, S. (2019). The economic burden of chronic obstructive pulmonary disease (COPD) in Europe: results from a systematic review of the literature. *The European Journal of Health Economics*, *21*(2), 181–194. https://doi.org/10.1007/s10198-019-01119-1

Rock, K. L., & Kono, H. (2008). The Inflammatory Response to Cell Death. *Annual Review of Pathology-Mechanisms of Disease*, *3*(1), 99–126. https://doi.org/10.1146/annurev.pathmechdis.3.121806.151456

Rosales Gerpe, M. C., Van Vloten, J. P., Santry, L. A., De Jong, J., Mould, R. C., Pelin, A., Bell, J. C., Bridle, B. W., & Wootton, S. K. (2018). Use of Precision-Cut Lung Slices as an *Ex vivo* Tool for Evaluating Viruses and Viral Vectors for Gene and Oncolytic Therapy. *Molecular Therapy - Methods &Amp; Clinical Development*, *10*, 245–256. https://doi.org/10.1016/j.omtm.2018.07.010

Rozenberg, J. M., Filkov, G. I., Trofimenko, A. V., Karpulevich, E. A., Parshin, V. D., Royuk, V. V., Sekacheva, M. I., & Durymanov, M. O. (2021). Biomedical Applications of Non-Small Cell Lung Cancer Spheroids. *Frontiers in Oncology*, *11*. https://doi.org/10.3389/fonc.2021.791069

Rudin, C. M., Brambilla, E., Faivre-Finn, C., & Sage, J. (2021). Small-cell lung cancer. *Nature Reviews Disease Primers*, *7*(1). https://doi.org/10.1038/s41572-020-00235-0

Russell, D. G. (2011). Mycobacterium tuberculosis and the intimate discourse of a chronic infection. *Immunological Reviews*, *240*(1), 252–268. https://doi.org/10.1111/j.1600-065x.2010.00984

Russell, R. E. K., Thorley, A., Culpitt, S. V., Dodd, S., Donnelly, L. E., Demattos, C., Fitzgerald, M., & Barnes, P. J. (**2002).** Alveolar macrophage-mediated elastolysis: roles of matrix metalloproteinases, cysteine, and serine proteases. *American Journal of Physiology-Lung Cellular and Molecular Physiology*, *283*(4), L867–L873. https://doi.org/10.1152/ajplung.00020.2002

Saeki, M., Nishimura, T., Kitamura, N., Hiroi, T., Mori, A., & Kaminuma, O. (2019). Potential Mechanisms of T Cell-Mediated and Eosinophil-Independent Bronchial Hyperresponsiveness. *International Journal of Molecular Sciences*, *20*(12), 2980. https://doi.org/10.3390/ijms20122980

Saeki, M., Nishimura, T., Kitamura, N., Hiroi, T., Mori, A., & Kaminuma, O. (2019). Potential Mechanisms of T Cell-Mediated and Eosinophil-Independent Bronchial Hyperresponsiveness. *International Journal of Molecular Sciences*, *20*(12), 2980. https://doi.org/10.3390/ijms20122980

Sakalem, M. E., De Sibio, M. T., da Costa, F. A. D. S., & de Oliveira, M. (2021). Historical evolution of spheroids and organoids, and possibilities of use in life sciences and medicine. *Biotechnology Journal*, *16*(5), 2000463. https://doi.org/10.1002/biot.202000463

Sanderson, M. J. (2011). Exploring lung physiology in health and disease with lung slices. *Pulmonary Pharmacology &Amp; Therapeutics*, *24*(5), 452–465. https://doi.org/10.1016/j.pupt.2011.05.001

Schabath, M. B., & Cote, M. L. (2019). Cancer Progress and Priorities: Lung Cancer. *Cancer Epidemiology, Biomarkers &Amp; Prevention*, *28*(10), 1563–1579. https://doi.org/10.1158/1055-9965.epi-19-0221

Sebina, I., & Phipps, S. (2020). The Contribution of Neutrophils to the Pathogenesis of RSV Bronchiolitis. *Viruses*, *12*(8), 808. https://doi.org/10.3390/v12080808

Shapouri-Moghaddam, A., Mohammadian, S., Vazini, H., Taghadosi, M., Esmaeili, S., Mardani, F., Seifi, B., Mohammadi, A., Afshari, J. T., & Sahebkar, A. (2018). Macrophage plasticity, polarization, and function in health and disease. *Journal of Cellular Physiology*, *233*(9), 6425–6440. https://doi.org/10.1002/jcp.26429

Shukla, S. D., Swaroop Vanka, K., Chavelier, A., Shastri, M. D., Tambuwala, M. M., Bakshi, H. A., Pabreja, K., Mahmood, M. Q., & O'Toole, R. F. (2020). Chronic respiratory diseases: An introduction and need for novel drug delivery approaches. *Targeting Chronic Inflammatory Lung Diseases Using Advanced Drug Delivery Systems*, 1–31. https://doi.org/10.1016/b978-0-12-820658-4.00001-7

Smith, N. H., Gordon, S. V., de la Rua-Domenech, R., Clifton-Hadley, R. S., & Hewinson, R. G. (2006). Bottlenecks and broomsticks: the molecular evolution of Mycobacterium bovis. *Nature Reviews Microbiology*, *4*(9), 670–681. https://doi.org/10.1038/nrmicro1472

Steinman, R. M., & Banchereau, J. (2007). Taking dendritic cells into medicine. *Nature*, *449*(7161), 419–426. https://doi.org/10.1038/nature06175

Suraya, R., Nagano, T., Katsurada, M., Sekiya, R., Kobayashi, K., & Nishimura, Y. (2021). Molecular mechanism of asthma and its novel molecular target therapeutic agent. *Respiratory Investigation*, *59*(3), 291–301. https://doi.org/10.1016/j.resinv.2020.12.007

Surolia, R., Li, F. J., Wang, Z., Li, H., Liu, G., Zhou, Y., Luckhardt, T., Bae, S., Liu, R. M., Rangarajan, S., de Andrade, J., Thannickal, V. J., & Antony, V. B. (2017). 3D pulmospheres serve as a personalized and predictive multicellular model for assessment of antifibrotic drugs. *JCI Insight*, *2*(2). https://doi.org/10.1172/jci.insight.91377

Temann, A., Golovina, T., Neuhaus, V., Thompson, C., Chichester, J. A., Braun, A., & Yusibov, V. (2016). Evaluation of inflammatory and immune responses in long-term cultured human precision-cut lung slices. *Human Vaccines &Amp; Immunotherapeutics*, *13*(2), 351–358. https://doi.org/10.1080/21645515.2017.1264794

Thacker, V. V., Dhar, N., Sharma, K., Barrile, R., Karalis, K., & McKinney, J. D. (2020). A lung-on-chip model of early Mycobacterium tuberculosis infection reveals an essential role

for alveolar epithelial cells in controlling bacterial growth. *ELife*, *9*. https://doi.org/10.7554/elife.59961

The Global Asthma Report 2022. (2022). *The International Journal of Tuberculosis and Lung Disease*, *26*(1), 1–104. https://doi.org/10.5588/ijtld.22.1010

Thomas, D. W., Burns, J., Audette, J., Carroll, A., Dow-Hygelund, C., & Hay, M. (2016). *Clinical Development Success Rates 2006-2015*. Biomedtracker, S. D. https://pharmaintelligence.informa.com/~/media/informa-shop-window/pharma/2021/files/reports/2021-clinical-development-success-rates-2011-2020-v17.pdf

Tomita, K., Barnes, P., & Adcock, I. (2003). The effect of oxidative stress on histone acetylation and IL-8 release. *Biochemical and Biophysical Research Communications*, *301*(2), 572–577. https://doi.org/10.1016/s0006-291x(02)03029-2

Torres, A., Cilloniz, C., Niederman, M. S., Menéndez, R., Chalmers, J. D., Wunderink, R. G., & van der Poll, T. (2021). Pneumonia. *Nature Reviews Disease Primers*, *7*(1). https://doi.org/10.1038/s41572-021-00259-0

Torres, A., Niederman, M. S., Chastre, J., Ewig, S., Fernandez-Vandellos, P., Hanberger, H., Kollef, M., Li Bassi, G., Luna, C. M., Martin-Loeches, I., Paiva, J. A., Read, R. C., Rigau, D., Timsit, J. F., Welte, T., & Wunderink, R. (2017). International ERS/ESICM/ESCMID/ALAT guidelines for the management of hospital-acquired pneumonia and ventilator-associated pneumonia. *European Respiratory Journal*, *50*(3), 1700582. https://doi.org/10.1183/13993003.00582-2017

Travis, W. D., Brambilla, E., Nicholson, A. G., Yatabe, Y., Austin, J. H., Beasley, M. B., Chirieac, L. R., Dacic, S., Duhig, E., Flieder, D. B., Geisinger, K., Hirsch, F. R., Ishikawa, Y., Kerr, K. M., Noguchi, M., Pelosi, G., Powell, C. A., Tsao, M. S., & Wistuba, I. (2015). The 2015 World Health Organization Classification of Lung Tumors. *Journal of Thoracic Oncology*, *10*(9), 1243–1260. https://doi.org/10.1097/jto.0000000000000630

Troeger, C., Blacker, B., Khalil, I. A., Rao, P. C., Cao, J., Zimsen, S. R. M., Albertson, S. B., Deshpande, A., Farag, T., Abebe, Z., Adetifa, I. M. O., Adhikari, T. B., Akibu, M., Al Lami, F. H., Al-Eyadhy, A., Alvis-Guzman, N., Amare, A. T., Amoako, Y. A., Antonio, C. A. T., . . . Reiner, R. C. (2018). Estimates of the global, regional, and national morbidity, mortality, and aetiologies of lower respiratory infections in 195 countries, 1990–2016: a systematic analysis for the Global Burden of Disease Study 2016. *The Lancet Infectious Diseases*, *18*(11), 1191–1210. https://doi.org/10.1016/s1473-3099(18)30310-4

Van Dijk, E. M., Culha, S., Menzen, M. H., Bidan, C. M., & Gosens, R. (2017). Elastase-Induced Parenchymal Disruption and Airway Hyper Responsiveness in Mouse Precision Cut Lung Slices: Toward an *Ex vivo* COPD Model. *Frontiers in Physiology*, *7*. https://doi.org/10.3389/fphys.2016.00657

Viana, F., O'Kane, C. M., & Schroeder, G. N. (2021). Precision-cut lung slices: A powerful *ex vivo* model to investigate respiratory infectious diseases. *Molecular Microbiology*, *117*(3), 578–588. https://doi.org/10.1111/mmi.14817

Wang, M., Zhou, T., Zhang, Z. P., Liu, H., Zheng, Z., & Xie, H. (2021). Current therapeutic strategies for respiratory diseases using mesenchymal stem cells. *MedComm*, *2*(3), 351–380. https://doi.org/10.1002/mco2.74

WCRF International. (2022, April 14). *Lung cancer statistics | World Cancer Research Fund International*. Retrieved December 20, 2022, from https://www.wcrf.org/cancer-trends/lung-cancer-statistics/

Wenzel, R. P., & Fowler, A. A. (2006). Acute Bronchitis. *New England Journal of Medicine*, *355*(20), 2125–2130. https://doi.org/10.1056/nejmcp061493

Wisnivesky, J., & de-Torres, J. P. (2019). The Global Burden of Pulmonary Diseases: Most Prevalent Problems and Opportunities for Improvement. *Annals of Global Health*, *85*(1). https://doi.org/10.5334/aogh.2411

World Health Organization. (2020). *Cancer today*. International Agency for Research on Cancer. Global Cancer Observatory: Cancer Today. Retrieved December 20, 2022, from https://gco.iarc.fr/today/online-analysis-multi-bars?v=2020

World Health Organization. (2020). *The top 10 causes of death*. https://www.who.int/news-room/fact-sheets/detail/the-top-10-causes-of-death

World Health Organization. (2022, May 20). *Chronic obstructive pulmonary disease (COPD)*. https://www.who.int/news-room/fact-sheets/detail/chronic-obstructive-pulmonary-disease-(copd)

World Health Organization. (2022, October 27). *Tuberculosis (TB)*. Retrieved December 14, 2022, from https://www.who.int/news-room/fact-sheets/detail/tuberculosis

World Health Organization. (2022a, February 3). *Cancer*. Retrieved December 20, 2022, from https://www.who.int/news-room/fact-sheets/detail/cancer

Worrall G. (2008). Acute bronchitis. *Canadian family physician Medecin de famille canadien*, *54*(2), 238–239.

Wu, X., Van Dijk, E. M., Bos, I., Kistemaker, L. E. M., & Gosens, R. (2019). Mouse Lung Tissue Slice Culture. *Methods in Molecular Biology*, 297–311. https://doi.org/10.1007/978-1-4939-9086-3_21

Yaqub, N., Wayne, G., Birchall, M., & Song, W. (2022). Recent advances in human respiratory epithelium models for drug discovery. *Biotechnology Advances*, *54*, 107832. https://doi.org/10.1016/j.biotechadv.2021.107832

Yuksel, H., Ocalan, M., & Yilmaz, O. (2021). E-Cadherin: An Important Functional Molecule at Respiratory Barrier Between Defence and Dysfunction. *Frontiers in Physiology*, *12*. https://doi.org/10.3389/fphys.2021.720227

Zanoni, M., Piccinini, F., Arienti, C., Zamagni, A., Santi, S., Polico, R., Bevilacqua, A., & Tesei, A. (2016). 3D tumor spheroid models for in vitro therapeutic screening: a systematic

approach to enhance the biological relevance of data obtained. *Scientific Reports*, *6*(1). https://doi.org/10.1038/srep19103

Zhang, M., Wang, P., Luo, R., Wang, Y., Li, Z., Guo, Y., Yao, Y., Li, M., Tao, T., Chen, W., Han, J., Liu, H., Cui, K., Zhang, X., Zheng, Y., & Qin, J. (2020). Biomimetic Human Disease Model of SARS-CoV-2-Induced Lung Injury and Immune Responses on Organ Chip System. *Advanced Science*, *8*(3), 2002928. https://doi.org/10.1002/advs.202002928

Zhang, M., Xu, C., Jiang, L., & Qin, J. (2018). A 3D human lung-on-a-chip model for nanotoxicity testing. *Toxicology Research*, *7*(6), 1048–1060. https://doi.org/10.1039/c8tx00156a

Zimniak, M., Kirschner, L., Hilpert, H., Geiger, N., Danov, O., Oberwinkler, H., Steinke, M., Sewald, K., Seibel, J., & Bodem, J. (2021). The serotonin reuptake inhibitor Fluoxetine inhibits SARS-CoV-2 in human lung tissue. *Scientific Reports*, *11*(1). https://doi.org/10.1038/s41598-021-85049-0

Zscheppang, K., Berg, J., Hedtrich, S., Verheyen, L., Wagner, D. E., Suttorp, N., Hippenstiel, S., & Hocke, A. C. (2017). Human Pulmonary 3D Models For Translational Research. *Biotechnology Journal*, *13*(1), 1700341. https://doi.org/10.1002/biot.201700341